# Evolution and interaction of damage modes in fabric-reinforced composites under dynamic flexural loading

HIMAYAT ULLAH, ANDY. R. HARLAND, VADIM.V. SILBERSCHMIDT*

*Wolfson School of Mechanical and Manufacturing Engineering, Loughborough University, Leicestershire, LE11 3TU, UK*

* Corresponding author: Ashby Road, Loughborough, Leics., LE11 3TU, UK.

Phone: +44 1509 227504. Fax: +44 1509 227502, E-mail: V.Silberschmidt@lboro.ac.uk

**Abstract**

In this paper, an experimental study is performed to characterise the behaviour of fabric-reinforced composites used in sports products under large-deflection bending in Izod-type impact tests. X-ray micro computed tomography (micro-CT) is used to investigate various damage modes in the impacted CFRP specimens. It revealed that matrix cracking, delaminations, tow debonding, and fibre fracture were the prominent damage modes. Three-dimensional finite-element models are developed to study the onset, progression and interaction of some damage modes such as delamination and fabric fracture observed with micro-CT. A damage modelling technique based on a cohesive-zone method, which is more efficient than continuum damage mechanics approach, is proposed for analysis of interaction of damage modes. The developed numerical models are capable to simulate the damage mechanisms and their interaction observed in the tests. In this study, the pattern of damage formation observed in specimens was front-to-back, unlike bottom-to-top one in drop weight impact tests. The effect of boundary conditions on the dynamic response and damage evolution of composite laminates is also investigated.

Keywords: A. Fabric, B. Impact behaviour, B. Delamination, B. Fracture, C. Modelling

## 1. Introduction

The application of woven composites such as carbon fabric-reinforced polymer (CFRP) and glass fabric-reinforced polymer (GFRP) laminates is ever increasing in impact-prone structures due to their better resistance to impact damage particularly delamination and fracture toughness than unidirectional tape laminates [1, 2]. Apart from aerospace and automotive structural elements, woven composites are also incorporated in design of sports products that could be subjected to large-deflection bending caused by dynamic loading. Composite structures such as aircraft wings, automotive bumpers and sports products e.g. athletic footwear insoles [3] and a custom-built Flex-Foot Cheetah blade for elite amputee athletes [4]

are subjected to large-deflection bending caused by low-velocity impacts during service. In contrast to traditional impact events such as bird strike or tool drop, kinematics, velocity and energy of large-deflection dynamic bending events are significantly different which cannot be replicated by drop weight testing where the flexure is significantly constrained; hence, should be properly studied. The damage mechanisms typically caused by impact loads in composite structures are matrix cracking, fibre breakage, delamination between adjacent layers and, ultimately, fabric fracture [5]. These damage modes are usually investigated with the use of 2D damage characterization techniques such as visual inspection, microscopy, radiography and ultrasonography, which are not adequate for analysis of inherently 3D damage processes within the composite laminates. Further, these conventional techniques are either destructive or do not provide a reasonable spatial resolution. These shortcomings can be alleviated with the application of non-destructive X-ray micro-CT technique, which can provide 3D images of internal realisation of damage mechanisms and their interaction in the composites with high resolution. This relatively recent technique has been used to investigate damage mechanisms in composites at micron scale [6-8]. Therefore, in this study, damage suffered by the composites under new types of loading regimes such as large-deflection dynamic bending experienced by various products in service was investigated using micro-CT.

The behaviour of fabric-reinforced composites subjected to low-velocity impact was widely studied in [2, 9-11] among others. However, majority of the work deals with the behaviour of composites studied with drop weight impact tests, usually causing penetration and perforation damage in impacted laminates in which flexure is significantly constrained. A large-deflection dynamic bending behaviour of composite structures which can be replicated by a pendulum-type impactor is rarely investigated. Further, the inter-ply delamination is usually analysed with cohesive-zone models (CZMs) [12, 13], whereas the intra-ply damage mechanisms are normally predicted using continuum damage mechanics (CDM) [5, 10]. As observed in recent studies, due to the homogenisation process in CDM models, key information on the coupling of multiple damage modes is lost at the macroscopic scale, resulting in inaccurate prediction of a crack path [14]. Advanced CZMs have the potential to couple directly the intra-ply and inter-ply cracks to achieve unification of crack initiation and propagation within a single approach. This damage-interaction modelling approach was adopted in [15, 16] by using cohesive-zone elements (CZEs) in numerical analysis of composite specimens' fracture in tension. This technique was also employed in [8, 17] to

simulate the damage interaction in fabric-reinforced composites subjected to large-deflection quasi-static bending. However, applications of the modelling approach for interacting damage modes to simulate the behaviour of woven composites subjected to dynamic bending are still limited.

In this work, the flexural behaviour of woven CFRP and GFRP laminates subjected to pendulum-type impacts is studied for various levels of impact energy. The development of predictive models for impact behaviour of composites depends on the qualitative assessment of damage modes within the material. For this purpose, micro-structural examination of tested CFRP laminates with the micro-CT technique identified location and type of inter- and intra-ply damage modes. Since multiple modes of damage were observed in CT images, this work addresses modelling of initiation, propagation and interaction of only two major modes - delamination and fabric fracture - in CFRP laminates under dynamic bending. Three-dimensional (3D) FE models were developed in Abaqus/Explicit for specimens damaged and fractured at various impact-energy levels by inserting CZEs at the identified crack locations. In this paper, analysis of large-deflection dynamic bending, CZM-based modelling of damage interaction and comparison of damage evolution in large-deflection bending and constrained bending like quasi drop weight test conditions are the main novel elements of the approach developed to study dynamic damage.

## 2. Experimental methods

### 2.1 Materials

The composites studied were laminates with two different types of fabrics made of carbon and glass fibres reinforcing thermoplastic polyurethane (TPU) matrix. The laminates were produced from 0°/90° prepregs in the form of four plies designated as $[0°,90°]_{2s}$, where 0° and 90° represent yarns in the warp and weft directions, respectively. The laminates had a 2/2 twill balanced and symmetric weaving pattern with a fibre volume fraction of 45%. As damage is sensitive to geometrical parameters of woven laminates such as the size and location of tows and resin within the laminate, thus, main parameters of the laminate and its constituents can be found in Table 1. The elastic constants of CFRP and GFRP determined from the quasi-static tests are presented in Table 2; details of the tests for characterisation of both types of materials are presented elsewhere [8, 17].

### 2.2 Dynamic testing

Dynamic bending tests in a low-velocity range from 1.5 m/s to 2 m/s were carried out according to the ASTM D 4812 standard using an instrumented pendulum-type CEAST Resil impactor as shown in Fig. 1.

Un-notched rectangular specimens of 40 mm length, 25 mm width and 1.0 mm thickness were prepared from CFRP and GFRP laminates. In the dynamic tests, the bottom of the cantilever-like specimen was fixed rigidly in the machine vice; whereas its upper 30 mm part was hit with striker of the pendulum hammer with a controlled level of initial energy, resulting in large-deflection bending of the specimen. The line of contact (impact) of the hammer's striking nose was kept away at a distance of 22 mm from the specimen's fixed support according to the standard (see Fig. 6a). A calibrated impact hammer with a mass of 0.6746 kg and a length of 0.3268 m was employed in this work. Impact tests were performed on CFRP and GFRP specimens at energy levels of 0.1 J – 0.6 J and 0.1 J – 1.1 J, respectively, to determine the fracture energy of the specimens. The impact-force signal was captured by a piezoelectric force transducer fixed to the hammer's striking nose. The signal was registered with a sampling frequency of 227 kHz, with up to 5000 data points recorded per impact test by the data acquisition system DAS 8000 connected to the Resil impact tester.

### 2.3 Discussion of experimental results

Typical transient response of CFRP specimens tested at six different energy levels is presented in Fig. 2. From these plots, it is clear that the slope and the peak load of the force-time (Fig. 2a) and force-deflection (Fig. 2b) curves increased with increase in the impact energy. The slope of force-deflection curves represents the contact stiffness, while the enclosed area under the curves gives the absorbed energy. The descending sections of the curves, where both the load and deflection decrease, represent rebounding of the hammer. Clearly, the area under the curves increased with impact energy indicating an increase in the energy absorbed by CFRP laminates. Energy absorption in composites is mainly through elastic strain energy, plastic deformation and formation of various damage modes [18]. In the materials under study, the TPU matrix material is highly compliant and usually absorbs more energy without causing any appreciable damage. At low energy levels, a linear increase of force with time is observed at the start of loading, representing a purely elastic undamaged response of the specimen. The loading and unloading portions of the force-time curves have a nearly symmetric parabolic shape up to 0.4 J (Fig. 2a), indicating that very little damage has occurred. As the impact energy was increased to 0.5 J, fluctuations in the force-time and force-deflection response could be observed before the peak load was reached. Such fluctuations associated with load drops are caused by internal initiation of damage such as delamination at low incident energy with an associated reduction in the specimen's stiffness [9]. As the load continued

increasing, the damage grew and multiple delaminations at different ply interfaces could occur. The force-time curve became unsymmetrical at 0.5 J with regard to its peak as can be seen in Fig. 2a. The dynamic curves showed more oscillations due to significant damage before the fabric fracture occurred at a higher impact energy of 0.6 J. In Fig. 2a, the fabric rupture is represented by a quick drop in impact force implying a momentary loss of contact between the hammer and specimen due to tensile fracture of fibers at the front face (impacted tension side) of the specimen.

The dynamic response of GFRP specimens tested at energy levels 0.1 J – 1.1 J is shown in Fig. 3. The material showed no significant damage up to 0.4 J. As the impact energy increased, a Hertzian failure can be observed at the start of the impact events beyond 0.8 J. The specimens tested at energies between 0.8 J – 1.1 J also exhibited a permanent bending-like deflection after testing (Fig. 3b), which may be due to the visco-elasto-plastic nature of the glass fibres apart from the TPU matrix. The plasticization of matrix played an important role in the resin-rich regions leading to local permanent deformations due to ductility of the TPU matrix. In these non-penetration impact events, the load drops are associated with both elastic and plastic deformations as well as damage initiation. At the higher energy levels, with the increase load, the specimens yielded, implying the onset of plastic deformation represented by the plateau at the top of the curves (Fig. 3b). Thus, the specimens underwent large deformations during loading and, subsequently, a snap-back during the rebound (with the striker slipping past the specimen), represented by the drops and kinks in Figs. 3a and b, respectively. These drops corresponded to the loss of contact between the hammer and the specimen for a short period of time during slippage/snap-back. Unlike the CFRP specimens, the peak loads remained almost the same with appreciable increase in the deformation of GFRP specimens at higher impact energies. It was also observed that the GFRP laminate required higher impact energies for specified damage and failure due to its greater capacity of storing elastic energy.

In the flexural dynamic tests, the energy levels required for the failure of thin laminates were lower than those in traditional drop-weight impact tests. The reason is that in the latter case all the edges of the specimens are usually fully clamped and, thus, higher in-plane membrane stresses and flexural rigidity are developed in thin composite plates. In contrast, in the Izod-type bending tests, with only one side of the specimen clamped and the rest free, membrane stresses is lower. Also, the specimen's thickness is small in comparison with its dimensions resulting in lower flexural rigidity. Obviously, flexural rigidity of the composite specimens depends on material's stiffness, their geometry (size) and boundary conditions.

Further, increasing material's thickness means stiffer and stronger specimens due to their higher flexural rigidity, resulting in higher impact energy for the specified damage initiation and propagation as observed in [5]. Hence, the decrease in flexural rigidity and stress-stiffening effect in the thin cantilevered specimens required lower energy for their deformation, initiation and propagation of damage and ultimate fracture.

In experimental tests of CFRP specimens, the contact duration remained almost the same with increase in the impact velocity (Fig. 2a). Such a response indicates that the material's behaviour is strain rate-independent under dynamic loading in fibre-dominated modes as was also observed in [19]. However, the on-axis GFRP specimens exhibited a rate-dependent behaviour as the contact duration increased with the impact energy (Fig. 3a). The peak loads for CFRP specimens were higher than those of GFRP at the corresponding energy levels due to the higher material's stiffness. The latter also resulted in lower contact duration for CFRP specimens than that for GFRP at the respective impact energy levels. However, GFRP composites did not exhibit a catastrophic fracture like CFRP composites but rather deformed permanently at higher impact energies (Fig. 3b). This means that although GFRP composites are less strong but they sustain higher impact energy before their collapse. It can be delineated from the dynamic tests' results that a required peak force can be obtained by varying impact velocity for a constant hammer mass; while a given impact duration can be obtained by choosing the appropriate material's stiffness. Thus, the qualitative behaviour of GFRP specimens was different to that of CFRP, especially at higher energy levels. In the next sections, the damage behaviour only of CFRP laminates is studied with micro-CT and FE simulations; its choice was based on its higher properties.

### 2.4. Damage Characterization

In this study, X-ray micro-CT measurements of tested CFRP specimens were carried out on XT H 225 X-ray scanner. The system consisted of an X-ray detector and an electronic X-ray source, creating 2D cross-sections of the sample. The source was a sealed X-ray tube operating at 25–225 kV with a 3 μm spot size. Following acquisition of tomographic data for the sample, a software program built a precise 3D map from 2D radiograph images by 'stacking' the individual slices on top of each other; this process is known as *reconstruction*. As denser materials absorb more X-rays than voids and air, this attenuation contrast allows detection and characterisation of cracks and flaws in tomographic images. Two small samples, one with dimensions 8.31 mm x 6.50 mm x 1.0 mm from the impact region and second 7.90 mm x 6.10 mm x

1.0 mm from the fractured region of the CFRP specimen tested at 0.6 J were prepared. Data for the samples was collected at 80 kV and 85 μA. Transmission X-ray images were acquired from 3600 rotation views over 360° of rotation (rotation step of 0.1º) for 3D reconstruction. The obtained data was reconstructed using CT-Pro software, and the analysis of the resulting 3D volumes was performed with the VG Studio Max 2.2 software to partition and highlight regions of interest.

The reconstructed tomographs of the CFRP specimen from the impact location tested at impact energy of 0.6 J are presented in Fig. 4. The images show matrix cracking, delamination and tow debonding at the hammer's impact location along the specimen's height. Dark-grey regions in images represent cracks and damage whereas light-grey areas represent a higher-density material, i.e. carbon-fibre tows. Damage initiation first started below the striker ends at the impact location as represented by dents in the tows in Fig. 4a. The damage then grew within the specimen as the impact force increased with time until the fabric fracture occurred at the cantilever support (vice) at maximum load. At the impact location (Fig. 4c), the interface on the impact side (specimen's front side) is more damaged, which is different to the conical pattern of damage from bottom-to-top in drop weight impact tests studied in [9, 11]. Unlike the drop-weight test conditions, here, the specimen acted as a cantilever beam subjected to large-deflection bending, where the front (top) plies experienced tensile stresses and the back (bottom) ones compressive stresses. The tensile stresses caused more damage on the specimen's impact (front) side than the compressive stresses on the non-impact (back) side. Damage in the middle plies was caused by the maximum interlaminar shear stress at the neutral plane of the specimen. Hence, such a stress distribution was responsible for the front-to-back (top-to-bottom) pattern of damage formation in the specimen. These observations are also corroborated by the stress distribution obtained through numerical analysis described below (see Fig. 13a). All the resin-rich interfaces underwent inter-ply delamination below the impactor. Further, in drop-weight impact specimens, the damage mode is usually dominated by contact and shear stresses causing penetration and perforation at the impact location; whereas, here in the dynamic bending, damage was dominated by a flexural-membrane stress in the tested specimens.

Figure 5 shows the reconstructed 3D images of the CFRP specimen at the bending (fractured) location. Realisation of inter-ply and intra-ply damage mechanisms at its outer edge, 25%, 50%, and 75% of the sample's width is shown in Figs. 5a, b, c, and d, respectively. It was shown that before ultimate fracture, the laminate exhibited matrix cracking and then delaminations and tow debondings near the specimen's

support. Matrix cracks developed in the weak resin-rich pockets around the tows. Inter-ply delamination and intra-ply delamination such as tow debonding can also be observed. These delaminations normally appeared near the matrix cracks regions, which suggested that formation of cracks initiated delamination. In the fibre-rich regions, damage was apparently linked to debonding at the fibre/matrix interface. Such damage is usually caused by the local stress concentrations at the tow/fibre crimps in woven composites under tensile loads. The analysis of internal structure showed that at the time of fabric fracture, which was triggered by tensile fibre failure, almost every ply was delaminated. This delamination is more pronounced in Figs. 5a and c than in 5b and d. The reason is that warp tows, which are aligned along the specimen's axis, bear a higher load than transverse weft tows in bending of the specimen under impact. All the tomographs showed that matrix cracking, delamination and tow debonding were the prominent damage modes at the specimen's impact location, whereas at the bending location, these modes were coupled with fabric fracture.

## 3. Numerical Simulations

The complex weaving architecture as well as multiple modes of damage at various length scales in woven composites makes the micro-mechanics-based constituent-level modelling more computationally expensive for a real-size problem. Thus, a meso-level modelling approach dealing with homogeneous orthotropic plies and a cohesive interface connecting two adjacent plies was adopted to investigate the macro-level response of specimens with dimensions used in tests. Such a meso-level approach coupled with CDM was used in [5, 10, 20] to analyse the damage behaviour of woven composite structures. Here, a discrete modelling approach based on the CZM rather than CDM is employed to realise the out–of-plane fabric fracture apart from the interface delamination and their interaction, without any compromise on the global behaviour of the structure. In the FE models, the material was assumed to have purely elastic orthotropic behavior before the damage initiation. Delamination damage and fabric fracture were assumed to be confined to interfaces, located between the predefined damageable regions, and through-thickness transverse straight cut at the specimen's fracture location, respectively. Both the impactor and the specimen were defined as deformable bodies in the contact interactions to simulate the real-world physics of the problem. A friction coefficient of 0.3 was assumed between the CFRP specimen and the steel hammer as used in [21].

### 3.1. Finite-element model

In this study, three 3D FE models – Models I, II and III as shown in Fig. 6 – were developed to simulate a dynamic behaviour of damaged and fractured CFRP specimens at impacts with energy levels 0.5 J and 0.6 J, respectively. In Model I of the damaged specimen at 0.5 J impact energy; CZEs were defined at the resin-rich interfaces between the laminate's plies. Hence, Model I contained three longitudinal cohesive layers - one in front of the beam's neutral plane (NP), the second coinciding with it, and the third to the back of the NP to simulate multiple delamination scenarios. Model II is similar to Model I except the top edge of the specimen is fully constrained to create the conditions of fixed-fixed specimen (quasi drop weight test simulation) under dynamic bending. Model II was developed to investigate the effect of boundary conditions on the damage evolution under dynamic loading. Model III (fractured specimen at 0.6 J) had, in addition to the same three interface layers of CZEs, one more through-thickness transverse cohesive layer placed at the specimen's fracture location, to model both the inter-ply delamination and intra-ply fabric fracture and their interaction. The following notation is used for cohesive layers in Models I, II and III: FCL - in front of the NP (towards impact face), MCL - the cohesive layer coinciding with the NP, and BCL - the one to the back of the NP; the through-thickness transverse layer is denoted as CCL. These cohesive layers were included in the model since the location of damage initiation is *a priori* known from the micro-CT analysis in this study. However, the location of damage initiation within a composite laminate can also be described analytically. Particularly, cohesive elements can be placed at interfaces between plies having different orientations, which are more prone to inter-ply delamination [14]. In addition, they can also be placed in matrix-dominated regions such as interfaces between the layers with the same orientation, especially at the mid-plane of the laminate, which are more susceptible to damage initiation due to their low interlaminar shear strength [5]. However, increasing the number of cohesive layers will increase the computational cost and the solution convergence may become rather complicated [13]. Since CFRP composites are essentially strain rate-independent in fibre-dominated modes such as on-axis $[0°,90°]_{2s}$ laminates subjected to in-plane tension and compression in the low-velocity (low strain-rate) regimes, the material constants obtained from the quasi-static tests (Table 2) were used in the FE models. Similarly, the cohesive law was assumed to be strain-rate insensitive, and thus static fracture-toughness values were assumed for a dynamic crack growth; this was proven to be sufficient in previous dynamic-fracture studies [22].

Cohesive-zone elements (CZEs) were used to model both the inter-ply and intra-ply damage modes and their interaction in CFRP laminates. The nominal quadratic stress criterion was used for damage initiation, whereas the Benzeggagh and Kenane criterion [23] was used for damage propagation. Parameters of the cohesive-zone elements presented in Table 3 were taken from the authors' previous work [17]. Apart from inter-ply damage modelling, CZEs have also been used to model intra-ply damage mechanisms such as splitting and ply fracture in composite laminates [16]. Here, the initiation of intra-ply fabric damage was linked to average ultimate flexural strength of 720 MPa in both warp and weft directions from the quasi-static bending tests. Intra-ply fracture evolution was based on fabric fracture energy of 40 kJ/m$^2$ in both warp and weft directions as reported in [10] for a similar carbon fabric. The stiffness of finite-thickness cohesive elements was calibrated according to $K = E_{33}/t_i$, proposed by Daudeville *et al.* [24], where $E_{33}$ (8 GPa) is the material's through-thickness stiffness and $t_i$ - 16 µm (taken from [25]) is the thickness of resin-rich interface between plies; resulting in interface stiffness of 5 x 10$^{14}$ N/m$^3$ for inter-ply damage. However, stiffness of the interface elements defined for intra-ply fracture was based on the longitudinal elastic stiffness $E_{11}$ of the ply instead of $E_{33}$ in the above relation resulting in a higher value of 1x10$^{15}$ N/m$^3$. Further details of the FE modelling such as the modelled test set-up, geometry, mesh and element types, and boundary conditions can be seen elsewhere [25].

### 3.2. Discussion of simulations results

#### 3.2.1. Response of damaged specimen

Comparison of the experimental and predicted force-time responses and evolution of damage at the impact location of of CFRP laminate in FE Model I at impact energy of 0.5 J is shown in Fig. 7. Fluctuations in the experimental force-time history designated as $F_d$ - Exp representing the internal damage initiation (load drops in Fig. 7) are observed before the peak load is reached. Apparently, both the global response and the contact duration are reasonably well predicted for the damaged specimen. However, the numerical damage threshold $F_d$ - FE, at which a significant change in the laminate stiffness was detected, was under-predicted in the FE model. This discrepancy might be due to the meso-level formulation for the plies in the model. Apparently, in experiments, the fabric-reinforced laminates absorbed more energy due to the ductile resin-rich pockets and the interlacing of fibres in two orthogonal directions, and, thus, offered more resistance to damage initiation, which were not taken into account in the simulations. However, in Fig. 7, the impact force and duration in numerical simulations are higher

than those in experiments, asserting higher energy dissipation in the FE model. This extra energy could be caused by an exaggerated amount of viscous dissipation in the model after damage initiation.

Similarly, the evolution of damage area at the impact location calculated with Model I is also plotted in Fig. 7. Figure 8 shows the calculated delamination area at three interfaces – FCL, MCL and BCL – in simulation with Model I at two different time intervals: at 3 ms (after $F_d$ - FE; Fig. 7) and at 6 ms (near peak load; Fig. 7). Here, delamination initiated first at the point of striker impact and then at the bending location of the cantilevered CFRP specimen. The ends of the trace were damaged more due to sharp corners of the hammer striker. A large and quick increase in the delamination area was observed simultaneously in all the layers beyond the time corresponding to $F_d$ - FE. It can be seen from both Figs. 7 and 8 that the largest area of delamination occurred at the mid-plane interface layer MCL due to the high level of through-thickness shear stress. Thus, a Mode-II type delamination initiated in the specimen's mid-region, where shear stress reached the interface shear strength, and grew more in MCL than FCL and BCL at the impact location. Similarly, the maximum bending stresses at the upper (front) and lower (back) plies were foremost responsible for damage formation at FCL and BCL of the specimen, especially at the bending location (Fig. 8). After the load peak was reached at 6 ms, the damage growth stopped in the unloading region of the load-time response (Fig. 7). The size and shape of the individual delaminations could not be compared to their experimental counterparts as such experimental results were not possible with the micro-CT for the full-scale specimen due to the requirement of field of view of the system. Also, due to the weaving architecture of the laminate, the spread of the damage is not in a 2D plane. Here, the in-situ quantification of various damage modes is either very cumbersome or non-feasible.

The main focus of the FE study is to compare and analyse the salient features of the dynamics and damage evolution in flexural (cantilevered) and quasi drop weight tests (two ends fixed) specimens. The load history and evolution of damage with time for Model II, where the specimen was constrained as a fixed-fixed beam, is presented in Fig. 9. The fixed-fixed boundary conditions increased the flexural rigidity of thin laminates resulting in a high peak of the impact force - 600 N, which is approximately 7.5 times more than that predicted with only one end fixed (cantilevered) specimen (see Fig. 7). The impact duration also reduced from 12 ms to 2.5 ms due to increased stiffness of the fixed-fixed specimen. Figure 10 shows the extent of delamination area at three interfaces – FCL, MCL and BCL – in simulations with Model II for fixed-fixed specimen at two different time intervals: at 0.2 ms (just at $F_d$ - FE; Fig. 9) and at

1.2 ms (near peak load; Fig. 9). Here, the damage pattern is also different due to the constraints. Due to the higher impact force, the extent and magnitude of damage at the impact location are higher especially near the constrained top edge than that shown in Fig. 8. Here, too, the MCL is more damaged at the impact location.

To investigate the effect of constraints on inter-ply damage evolution, comparison of damage progression in both Models I and II with cantilevered and both ends fixed (quasi drop weight, qDW) conditions, respectively, is presented in Fig. 11. The rate of damage growth in quasi drop weight specimen is faster than that of cantilevered one. This demonstrates that due to both ends fixed, the specimen of the same size under similar impact energy of 0.5 J dissipates a lot of energy very quickly than the cantilevered specimen in Model I. Further, the extent of damage is also higher in quasi drop weight model in all interface layers than that of cantilevered specimen. Here, it can be inferred from these results that the boundary conditions of the specimens has not only a significant effect on the impact force and duration but also on the damage evolution within the specimen.

**3.3.2. Response of fractured specimen**

Fabric fracture occurred as the impact energy was increased to 0.6 J in experimental tests. The predicted evolution of impact force in Model III is compared with experimental results at this level of energy in Fig. 12. Here, too, the load drops designated as $F_d$ - Exp and $F_d$ - FE represents delamination initiation for the experiments and numerical results, respectively. The experimental curve shows more fluctuations due to significant damage after the damage threshold $F_d$ - Exp at higher impact energy, followed by the ultimate ply fracture at 4.8 ms. The final ply fracture is presented by a sudden drop in the impact force; however, the load didn't drop to zero, because in dynamic bending the distal plies in compression were not fractured causing a residual load of about 22 N. The simulation showed the ply fracture somewhat earlier - at 4.38 ms, which might be due to the low ply fracture initiation strength defined in Model III. Still, the FE analysis gave a good prediction of the important characteristics of the failure process.

The sequence of inter-ply delamination and intra-ply fabric breakage as well as their interaction in Model III is illustrated in the deformed contour plots for flexural stress $\sigma_{11}$ shown in Fig. 13. Although the laminate was fully delaminated in Fig. 13a, the flexural stress contours were almost uniform. The stress reduced as the first ply's fracture occurred at 4.38 ms as shown in Fig. 13b followed by fracture of the second ply in Figs. 13c at 4.62 ms. The third and fourth plies remained intact because of compressive

stresses on back side of the specimen in the bending. These plies carried the residual load and were in tension and compression states, respectively, as can be seen in Figs. 13c and d. Stress concentration at the locations of inter-ply and intra-ply crack tips is apparent in Figs. 13b-d. As the load increased, the ply elements moved relative to each other as in Mode-II type fracture along the delaminated interface layers as shown in Fig. 13d. There may be the possibility of fibre kinking due to buckling instability in the back plies under compression; however, this behaviour is not studied in the meso-scale models.

## 4. Conclusions

The behaviour of fabric-reinforced composites under dynamic bending was studied using experimental tests, micro-CT scanning and numerical simulations. The dynamic tests revealed that the CFRP laminates were fractured at lower energy levels than GFRP due to their lower energy absorbing capability. However, the impact strength of the CFRP laminates was higher than that of GFRP. Further, on-axis GFRP laminates exhibited a strain-rate sensitive behaviour as compared to CFRP specimens. In the impact bending tests, the specimens failed at lower impact energy as compared to their failure in drop weight impact tests. It was also found that damage in the specimens at the impact location was from its front to the back in the large-deflection impact tests, unlike the bottom-to-top character in drop weight tests. Considerable matrix cracking leading to tow debonding and delamination was observed along with tow fibre fracture in the micro-CT scanning of the impacted CFRP laminates. This microstructural characterisation formed a basis for damage incorporation in the developed 3D FE models.

The results of meso-scale 3D FE models of CFRP laminates were close to the experimental ones, and, the simulations were capable to reproduce the damage sequence and patterns observed experimentally. The numerical models helped to offer significant information about the complex damage phenomena that occurred at various stages of impact bending. For instance, interaction of delamination and ply fracture, which cannot be assessed directly in real tests and by non-destructive investigation, was captured with the CZM-based modelling approach. Similarly, the effect of boundary conditions on the dynamic response was also predicted for the first time, which is hard to obtain experimentally for the fixed-fixed conditions. Such conditions resulted in an increased flexural rigidity of the impacted specimen and the higher peak load and reduced impact duration. These quasi drop weight test conditions also resulted in a larger extent of damage with a faster growth rate. This also corroborated our observations that cantilever specimens failed at lower impact energies than fully clamped specimens in drop weight impact tests.

**References**

[1] Sutcliffe MPF, Monroy Aceves C, Stronge WJ, Choudhry RS, Scott AE. Moderate speed impact damage to 2D-braided glass–carbon composites. Composite Structures. 2012;94(5):1781-1792.

[2] Naik N, Chandra Sekher Y, Meduri S. Damage in woven-fabric composites subjected to low-velocity impact. Composites Science and Technology. 2000;60(5):731-744.

[3] Crabtree P, Dhokia V, Newman S, Ansell M. Manufacturing methodology for personalised symptom-specific sports insoles. Robotics and Computer-Integrated Manufacturing. 2009;25(6):972-979.

[4] http://www.ossur.com. 2013.

[5] Menna C, Asprone D, Caprino G, Lopresto V, Prota A. Numerical simulation of impact tests on GFRP composite laminates. International Journal of Impact Engineering. 2011;38(8–9):677-685.

[6] Scott A, Mavrogordato M, Wright P, Sinclair I, Spearing S. In situ fibre fracture measurement in carbon–epoxy laminates using high resolution computed tomography. Composites Science and Technology. 2011;71(12):1471-1477.

[7] Sket F, Seltzer R, Molina-Aldareguía J, Gonzalez C, LLorca J. Determination of damage micromechanisms and fracture resistance of glass fiber/epoxy cross-ply laminate by means of X-ray computed microtomography. Composites Science and Technology. 2012;72:350-359.

[8] Ullah H, Harland A, Silberschmidt V. Experimental and Numerical Analysis of Damage in Woven GFRP Composites Under Large-deflection Bending. Applied Composite Materials. 2012;19(5):769-783.

[9] Aktaş M, Ersen Balcıoğlu H, Aktaş A, Türker E, Emin Deniz M. Impact and post impact behavior of layer fabric composites. Composite Structures. 2012;94:2809-2818.

[10] Iannucci L, Willows M. An energy based damage mechanics approach to modelling impact onto woven composite materials--Part I: Numerical models. Composites Part A: Applied Science and Manufacturing. 2006;37(11):2041-2056.

[11] Kim JK, Sham ML. Impact and delamination failure of woven-fabric composites. Composites Science and Technology. 2000;60(5):745-761.

[12] Wisnom MR, Hallett SR. The role of delamination in strength, failure mechanism and hole size effect in open hole tensile tests on quasi-isotropic laminates. Composites Part A. 2009;40(4):335-342.

[13] Ullah H, Harland AR, Lucas T, Price D, Silberschmidt VV. Finite-element modelling of bending of CFRP laminates: Multiple delaminations. Computational Materials Science. 2012;52(1):147-156.

[14] Wisnom MR. Modelling discrete failures in composites with interface elements. Composites Part A. 2010;41(7):795-805.

[15] Fang XJ, Zhou ZQ, Cox BN, Yang QD. High-fidelity simulations of multiple fracture processes in a laminated composite in tension. Journal of the Mechanics and Physics of Solids. 2011;59(7):1355-1373.

[16] Hallett SR, Jiang WG, Khan B, Wisnom MR. Modelling the interaction between matrix cracks and delamination damage in scaled quasi-isotropic specimens. Composites Science and Technology. 2008;68(1):80-89.

[17] Ullah H, Harland AR, Silberschmidt VV. Damage modelling in woven-fabric CFRP laminates under large-deflection bending. Computational Materials Science. 2012;64:130-135.

[18] Hosur M, Adbullah M, Jeelani S. Studies on the low-velocity impact response of woven hybrid composites. Composite Structures. 2005;67(3):253-262.

[19] López-Puente J, Li S. Analysis of strain rate sensitivity of carbon/epoxy woven composites. International Journal of Impact Engineering. 2012;48(0):54-64.

[20] Sokolinsky VS, Indermuehle KC, Hurtado JA. Numerical simulation of the crushing process of a corrugated composite plate. Composites Part A: Applied Science and Manufacturing. 2011;42:1119-1126.

[21] Lopes C, Camanho P, Gürdal Z, Maimí P, González E. Low-velocity impact damage on dispersed stacking sequence laminates. Part II: Numerical simulations. Composites Science and Technology. 2009;69(7-8):937-947.

[22] Gözlüklü B, Coker D. Modeling of the dynamic delamination of L-shaped unidirectional laminated composites. Composite Structures. 2012;94(4):1430-1442.

[23] Benzeggagh ML, Kenane M. Measurement of mixed-mode delamination fracture toughness of unidirectional glass/epoxy composites with mixed-mode bending apparatus. Composites Science and Technology. 1996;56(4):439-449.

[24] Daudeville L, Allix O, Ladeveze P. Delamination analysis by damage mechanics: some applications. Composites Engineering. 1995;5(1):17-24.

[25] Ullah H, Harland AR, Silberschmidt VV. Damage and fracture in carbon fabric reinforced composites under impact bending. Composite Structures. 2013;101(0):144-156.

**Figure Captions**

Fig. 1. Resil impact test set-up

Fig. 2. Experimental response of twill 2/2 CFRP laminates at various impact energies: (a) force-time curves; (b) force-deflection curves

Fig. 3. Experimental response of twill 2/2 GFRP laminates at various impact energies: (a) force-time curves; (b) force-deflection curves

Fig. 4. Reconstructed 3D tomographs of twill 2/2 CFRP specimen at impact location across height of sample (resolution 6.7 μm): (a) edge; (b) 25% (1 mm above impact centre line) (c) 50% (at impact centre); (d) 75% (below impact centre line) of height

Fig. 5. Reconstructed 3D tomographs of twill 2/2 CFRP specimen at bending (fracture) location across width of sample (resolution 6.1 μm): (a) edge; (b) 25%; (c) 50%; (d) 75% of width

Fig. 6. Schematics of FE models for cantilever bending (Model I) (a), fixed-fixed bending ( quasi drop weight test simulation) (Model II) (b) and fractured (Model III) (c) behaviours of CFRP specimens tested at 0.5 J and 0.6 J impact energy, respectively

Fig. 7. Comparison of experimental and numerical force-time response and evolution of inter-ply delamination area at the impact location of CFRP laminate in FE Model I at impact energy of 0.5 J

Fig. 8. Delamination evolution in FE Model I at impact energy of 0.5 J at 3 ms (a) and 6 ms (b) [25]

Fig. 9. Numerical force-time response and damage evolution in FE Model II with fixed-fixed boundary (quasi drop weight (qDW) test) conditions at impact energy of 0.5 J

Fig. 10. Delamination evolution in FE Model II with fixed-fixed boundary conditions of the specimen at impact energy of 0.5 J at 0.2 ms (a) and 1.2 ms (b)

Fig. 11. Comparison of damage evolution under cantilever (flexural) and fixed-fixed (qDW) conditions of CFRP laminates from FE Models I and II at 0.5 J impact energy, respectively

Fig. 12. Comparison of experimental and numerical (Model III) force-time response for CFRP laminates at impact energy of 0.6 J

Fig. 13. Contours of bending stress $\sigma_{11}$ in Model III showing interaction of inter-ply and intra-ply damage at impact energy of 0.6 J at 4.2 ms (a), 4.38 ms (b), 4.62 ms (c) and 6.0 ms (d) (side view; scaling factor 0.5; fractured interfaces are represented by white colour)

**Table captions**

Table 1. Parameters of twill 2/2 woven composites

Table 2. Material properties of twill 2/2 woven composites

Table 3. Material parameters of inter-ply cohesive elements

Elsevier Editorial System(tm) for Composites Science and Technology
Manuscript Draft

Manuscript Number: CSTE-D-13-00764R1

Title: Evolution and interaction of damage modes in fabric-reinforced composites under dynamic flexural loading

Article Type: Full Length Article

Section/Category: Mechanics, modelling and analysis

Keywords: A. Fabric, B. Impact behaviour, B. Delamination, B. Fracture, C. Modelling

Corresponding Author: Professor Vadim V Silberschmidt,

Corresponding Author's Institution: Loughborough University

First Author: Himayat Ullah, Dr

Order of Authors: Himayat Ullah, Dr; Andy R Harland, Dr; Vadim V Silberschmidt

Abstract: In this paper, an experimental study is performed to characterise the behaviour of fabric-reinforced composites used in sports products under large-deflection bending in Izod-type impact tests. X-ray micro computed tomography (micro-CT) is used to investigate various damage modes in the impacted CFRP specimens. It revealed that matrix cracking, delaminations, tow debonding, and fibre fracture were the prominent damage modes. Three-dimensional finite-element models are developed to study the onset, progression and interaction of some damage modes such as delamination and fabric fracture observed with micro-CT. A damage modelling technique based on a cohesive-zone method, which is more efficient than continuum damage mechanics approach, is proposed for analysis of interaction of damage modes. The developed numerical models are capable to simulate the damage mechanisms and their interaction observed in the tests. In this study, the pattern of damage formation observed in specimens was front-to-back, unlike bottom-to-top one in drop weight impact tests. The effect of boundary conditions on the dynamic response and damage evolution of composite laminates is also investigated.

**Cover Letter**

Professor Marino Quaresimin
Regional Editor
Composites Science and Technology

Ms. Ref. No.: CSTE-D-13-00764
Title: Evolution and interaction of damage modes in fabric-reinforced composites under dynamic flexural loading

Re: Revision of manuscript

Dear Marino,

I am happy to submit a revised version of our paper titled “Evolution and interaction of damage modes in fabric-reinforced composites under dynamic flexural loading”, to your journal *Composites Science and Technology*. The manuscript was re-worked thoroughly, with all the comments of referees considered and addressed. The respective changes are highlighted in the file submitted with the revised manuscript.

Best regards,

Vadim
on behalf of the authors

---

Vadim V. Silberschmidt FIMechE FInstP
Professor of Mechanics of Materials
Associate Dean (Research)
ICoVIS Director
Head, Mechanics of Advanced Materials Research Group
Wolfson School of Mechanical and Manufacturing Engineering
Loughborough University
Loughborough Leicestershire LE11 3TU, U.K.
Phone: +44/(0)1509/227504
Fax: +44/(0)1509/227502

# Responses to Reviewers' Comments

Ms. Ref. No.: CSTE-D-13-00764
Title: ***Evolution and interaction of damage modes in fabric-reinforced composites under dynamic flexural loading***

The authors are grateful for interest of the reviewers to the manuscript and their helpful comments. The manuscript was re-worked thoroughly, with all the comments of reviewers considered and addressed. Details on the respective points and introduced revisions are given below:

**Reviewer #1:**

First of all I would like to thank the authors for the very interesting paper. In my opinion, the paper is really clear written and full of details and useful results.

Comment 1: Just for curiosity I would like to ask why the adopted energies are so low.

Authors' Response:

In the dynamic flexural tests, the energy levels required for the failure of thin laminates were lower than those for drop-weight impact tests. The reason is that in the latter tests all the edges of the specimens are usually fully clamped, resulting in higher in-plane membrane stresses and flexural rigidity in thin composite plates. In contrast, in the Izod-type bending tests presented in the paper, with only one side of the specimen clamped and the rest free, membrane stresses are lower. These conditions result in lower flexural rigidity and stress-stiffening effect in thin specimens, requiring lower energies for their deformation and damage initiation, propagation and ultimate fracture. That is why the adopted energies were lower than those in drop-weight impact tests of the specimens of the same size. This is elaborated in the respective section of the manuscript.

Comment 2: Second, I would like to suggest to introduce a schematic view better explain the dynamic tests carried out (paragraph 2.2).

Authors' Response:

A schematic of the dynamic test set-up is now presented in Fig.1.

Comment 3: About fig. 6, I suggest to check since it seems the contrary of what asserted about the absorbed energy at the beginning of paragraph 3.2.1.

Authors' Response:

In Fig. 6 (now Fig. 7), the impact force and duration of numerical simulation are higher than the experimental one, asserting higher energy dissipation in the FE model. This extra energy is assumed to be caused by an exaggerated amount of viscous dissipation in the model after damage initiation. The respective part is updated.

**Reviewer #2:**

Damage evolution studies in balanced symmetric laminated composites made of twill weave fabric under dynamic flexural loading with large deflection bending are presented. Studies are performed on GFRP and CFRP composites. Experimental studies are carried out using pendulum type impactor and X-ray micro-CT technique. Numerical studies are performed using 3D FEA and cohesive zone model. Finally, effect of boundary conditions on the dynamic response and damage evolution in laminated composites is investigated.

Damage modes considered are matrix cracking, delamination, tow debonding, inter-tow debonding and ply fracture.

**Experimental study:**

Comment 1: From practical application point of view, damage initiation studies are more important, Mode of damage and location of damage should be clearly identified, Is the damage initiation at the location of impact or some distance away from it?

Authors' Response:

The description of damage analysis is now rearranged according to the order of damage initiation and evolution in the specimen. The damage initiation is at the location of impact and then grows within the laminate with time. At the maximum load, ultimate fracture of the specimen occurs.

Comment 2: Is the location of damage initiation and location of fabric fracture the same?

Authors' Response:

The damage initiation first occurs below the ends of the striker at the impact location, whereas the fabric fracture occurs at the specimen's support (cantilever) vice. This is now clarified in the manuscript.

Comment 3: What is the co-relation between impact parameters, geometry and mechanical properties of the specimen and locations of damage initiation and ply fracture? Is the qualitative behaviour of GFRP and CFRP the same?

Is the qualitative behaviour of GFRP and CFRP the same?

Authors' Response:

The co-relation between impact parameters, geometry and mechanical properties of the specimen and locations of damage initiation and ply fracture for both CFRP and GFRP is described in last paragraph of Section 2.3.

Some elements of such a description are also given at the end of the first paragraph of Section 2.3. The qualitative behaviour of both the GFRP and CFRP specimens is different especially at higher energy levels. This description is now added in the manuscript.

Comment 4: ". pattern of damage formation observed in the specimens was front-to-back ..". This should be explained based on stress state in the specimen.

Authors' Response:

The respective section of the manuscript is now updated.

Comment 5: Figure 2: Physical explanation should be provided for the trend presented, especially at higher impact energies.

Authors' Response:

This description is now added in the manuscript.

**Numerical Study:**

Comment 6: Page 8, last 2 lines ".. location of damage initiation was a priori known from the micro-CT analysis." For numerical/analytical studies, a method should be worked out to predict the location of damage initiation.

Authors' Response:

The authors agree with the reviewer that it is not necessary to know *a priori* the location of damage initiation. Usually, cohesive elements should be placed at interfaces between plies having different orientations, which are more prone to inter-ply delamination. In addition, they can also be placed in matrix-dominated regions such as interfaces between layers with the same orientation, especially at the mid-plane of the laminate, which are more susceptible to damage initiation due to their low interlaminar shear strength. However, increasing the number of cohesive layers will increase the computational cost and the solution convergence may become rather complicated. The manuscript is modified accordingly.

Comment 7: Page 11, para 2, last two lines " boundary conditions of the

specimens have a significant effect ..." This is obvious. It is a separate issue, not related to the objective of the work presented.

Authors' Response:

The main objective of the work is the study of damage evolution in composites experimentally and numerically. However, the effect of boundary conditions on the damage evolution under dynamic loading was also investigated. For this purpose, FE Model II was developed where the top edge of the specimen was fully constrained to create the conditions of fixed-fixed specimen (quasi-drop-weight test simulation) under dynamic bending. Such conditions of fixing and loading were not possible experimentally with the Izod test set-up. The results of both Model I with the cantilever-type boundary conditions and Model II with the fixed-fixed conditions were compared in Fig.11.

Comment 8: For the effective comparison of experimental and numerical results, boundary conditions should be the same in numerical and experimental studies.

Authors' Response:

The authors agree with the reviewer that for the effective comparison of experimental and numerical results, boundary conditions should be the same in numerical and experimental studies. That is why the experimental and numerical response of CFRP specimens at impact energies of 0.5 J and 0.6 J were compared in Figs. 7 and 12, respectively, under the same cantilever-type boundary conditions. Since the fixed-fixed (qDW) conditions of the specimen are hard to obtain experimentally, such behaviour is studied only numerically. Hence, the damage evolution under cantilever (flexural) and fixed-fixed conditions from FE Models I and II at 0.5 J impact energy was compared in Fig. 11, to observe the effect of boundary conditions on damage evolution.

Comment 9: Assumptions made in numerical studies and justification for it should be included.

Authors' Response:

Assumptions made in the numerical studies along with their justifications are now included in the manuscript.

Vadim Silberschmidt
on behalf of the authors

# Evolution and interaction of damage modes in fabric-reinforced composites under dynamic flexural loading

HIMAYAT ULLAH, ANDY. R. HARLAND, VADIM.V. SILBERSCHMIDT*

*Wolfson School of Mechanical and Manufacturing Engineering, Loughborough University, Leicestershire, LE11 3TU, UK*

* Corresponding author: Ashby Road, Loughborough, Leics., LE11 3TU, UK.

Phone: +44 1509 227504. Fax: +44 1509 227502, E-mail: V.Silberschmidt@lboro.ac.uk

**Abstract**

In this paper, an experimental study is performed to characterise the behaviour of fabric-reinforced composites used in sports products under large-deflection bending in Izod-type impact tests. X-ray micro computed tomography (micro-CT) is used to investigate various damage modes in the impacted CFRP specimens. It revealed that matrix cracking, delaminations, tow debonding, and fibre fracture were the prominent damage modes. Three-dimensional finite-element models are developed to study the onset, progression and interaction of some damage modes such as delamination and fabric fracture observed with micro-CT. A damage modelling technique based on a cohesive-zone method, which is more efficient than continuum damage mechanics approach, is proposed for analysis of interaction of damage modes. The developed numerical models are capable to simulate the damage mechanisms and their interaction observed in the tests. In this study, the pattern of damage formation observed in specimens was front-to-back, unlike bottom-to-top one in drop weight impact tests. The effect of boundary conditions on the dynamic response and damage evolution of composite laminates is also investigated.

Keywords: A. Fabric, B. Impact behaviour, B. Delamination, B. Fracture, C. Modelling

## 1. Introduction

The application of woven composites such as carbon fabric-reinforced polymer (CFRP) and glass fabric-reinforced polymer (GFRP) laminates is ever increasing in impact-prone structures due to their better resistance to impact damage particularly delamination and fracture toughness than unidirectional tape laminates [1, 2]. Apart from aerospace and automotive structural elements, woven composites are also incorporated in design of sports products that could be subjected to large-deflection bending caused by dynamic loading. Composite structures such as aircraft wings, automotive bumpers and sports products e.g. athletic footwear insoles [3] and a custom-built Flex-Foot Cheetah blade for elite amputee athletes [4]

are subjected to large-deflection bending caused by low-velocity impacts during service. In contrast to traditional impact events such as bird strike or tool drop, kinematics, velocity and energy of large-deflection dynamic bending events are significantly different which cannot be replicated by drop weight testing where the flexure is significantly constrained; hence, should be properly studied. The damage mechanisms typically caused by impact loads in composite structures are matrix cracking, fibre breakage, delamination between adjacent layers and, ultimately, fabric fracture [5]. These damage modes are usually investigated with the use of 2D damage characterization techniques such as visual inspection, microscopy, radiography and ultrasonography, which are not adequate for analysis of inherently 3D damage processes within the composite laminates. Further, these conventional techniques are either destructive or do not provide a reasonable spatial resolution. These shortcomings can be alleviated with the application of non-destructive X-ray micro-CT technique, which can provide 3D images of internal realisation of damage mechanisms and their interaction in the composites with high resolution. This relatively recent technique has been used to investigate damage mechanisms in composites at micron scale [6-8]. Therefore, in this study, damage suffered by the composites under new types of loading regimes such as large-deflection dynamic bending experienced by various products in service was investigated using micro-CT.

The behaviour of fabric-reinforced composites subjected to low-velocity impact was widely studied in [2, 9-11] among others. However, majority of the work deals with the behaviour of composites studied with drop weight impact tests, usually causing penetration and perforation damage in impacted laminates in which flexure is significantly constrained. A large-deflection dynamic bending behaviour of composite structures which can be replicated by a pendulum-type impactor is rarely investigated. Further, the inter-ply delamination is usually analysed with cohesive-zone models (CZMs) [12, 13], whereas the intra-ply damage mechanisms are normally predicted using continuum damage mechanics (CDM) [5, 10]. As observed in recent studies, due to the homogenisation process in CDM models, key information on the coupling of multiple damage modes is lost at the macroscopic scale, resulting in inaccurate prediction of a crack path [14]. Advanced CZMs have the potential to couple directly the intra-ply and inter-ply cracks to achieve unification of crack initiation and propagation within a single approach. This damage-interaction modelling approach was adopted in [15, 16] by using cohesive-zone elements (CZEs) in numerical analysis of composite specimens' fracture in tension. This technique was also employed in [8, 17] to

simulate the damage interaction in fabric-reinforced composites subjected to large-deflection quasi-static bending. However, applications of the modelling approach for interacting damage modes to simulate the behaviour of woven composites subjected to dynamic bending are still limited.

In this work, the flexural behaviour of woven CFRP and GFRP laminates subjected to pendulum-type impacts is studied for various levels of impact energy. The development of predictive models for impact behaviour of composites depends on the qualitative assessment of damage modes within the material. For this purpose, micro-structural examination of tested CFRP laminates with the micro-CT technique identified location and type of inter- and intra-ply damage modes. Since multiple modes of damage were observed in CT images, this work addresses modelling of initiation, propagation and interaction of only two major modes - delamination and fabric fracture - in CFRP laminates under dynamic bending. Three-dimensional (3D) FE models were developed in Abaqus/Explicit for specimens damaged and fractured at various impact-energy levels by inserting CZEs at the identified crack locations. In this paper, analysis of large-deflection dynamic bending, CZM-based modelling of damage interaction and comparison of damage evolution in large-deflection bending and constrained bending like quasi drop weight test conditions are the main novel elements of the approach developed to study dynamic damage.

## 2. Experimental methods

### 2.1 Materials

The composites studied were laminates with two different types of fabrics made of carbon and glass fibres reinforcing thermoplastic polyurethane (TPU) matrix. The laminates were produced from 0°/90° prepregs in the form of four plies designated as $[0°,90°]_{2s}$, where 0° and 90° represent yarns in the warp and weft directions, respectively. The laminates had a 2/2 twill balanced and symmetric weaving pattern with a fibre volume fraction of 45%. As damage is sensitive to geometrical parameters of woven laminates such as the size and location of tows and resin within the laminate, thus, main parameters of the laminate and its constituents can be found in Table 1. The elastic constants of CFRP and GFRP determined from the quasi-static tests are presented in Table 2; details of the tests for characterisation of both types of materials are presented elsewhere [8, 17].

### 2.2 Dynamic testing

Dynamic bending tests in a low-velocity range from 1.5 m/s to 2 m/s were carried out according to the ASTM D 4812 standard using an instrumented pendulum-type CEAST Resil impactor as shown in Fig. 1.

Un-notched rectangular specimens of 40 mm length, 25 mm width and 1.0 mm thickness were prepared from CFRP and GFRP laminates. In the dynamic tests, the bottom of the cantilever-like specimen was fixed rigidly in the machine vice; whereas its upper 30 mm part was hit with striker of the pendulum hammer with a controlled level of initial energy, resulting in large-deflection bending of the specimen. The line of contact (impact) of the hammer's striking nose was kept away at a distance of 22 mm from the specimen's fixed support according to the standard (see Fig. 6a). A calibrated impact hammer with a mass of 0.6746 kg and a length of 0.3268 m was employed in this work. Impact tests were performed on CFRP and GFRP specimens at energy levels of 0.1 J – 0.6 J and 0.1 J – 1.1 J, respectively, to determine the fracture energy of the specimens. The impact-force signal was captured by a piezoelectric force transducer fixed to the hammer's striking nose. The signal was registered with a sampling frequency of 227 kHz, with up to 5000 data points recorded per impact test by the data acquisition system DAS 8000 connected to the Resil impact tester.

### 2.3 Discussion of experimental results

Typical transient response of CFRP specimens tested at six different energy levels is presented in Fig. 2. From these plots, it is clear that the slope and the peak load of the force-time (Fig. 2a) and force-deflection (Fig. 2b) curves increased with increase in the impact energy. The slope of force-deflection curves represents the contact stiffness, while the enclosed area under the curves gives the absorbed energy. The descending sections of the curves, where both the load and deflection decrease, represent rebounding of the hammer. Clearly, the area under the curves increased with impact energy indicating an increase in the energy absorbed by CFRP laminates. Energy absorption in composites is mainly through elastic strain energy, plastic deformation and formation of various damage modes [18]. In the materials under study, the TPU matrix material is highly compliant and usually absorbs more energy without causing any appreciable damage. At low energy levels, a linear increase of force with time is observed at the start of loading, representing a purely elastic undamaged response of the specimen. The loading and unloading portions of the force-time curves have a nearly symmetric parabolic shape up to 0.4 J (Fig. 2a), indicating that very little damage has occurred. As the impact energy was increased to 0.5 J, fluctuations in the force-time and force-deflection response could be observed before the peak load was reached. Such fluctuations associated with load drops are caused by internal initiation of damage such as delamination at low incident energy with an associated reduction in the specimen's stiffness [9]. As the load continued

increasing, the damage grew and multiple delaminations at different ply interfaces could occur. The force-time curve became unsymmetrical at 0.5 J with regard to its peak as can be seen in Fig. 2a. The dynamic curves showed more oscillations due to significant damage before the fabric fracture occurred at a higher impact energy of 0.6 J. In Fig. 2a, the fabric rupture is represented by a quick drop in impact force implying a momentary loss of contact between the hammer and specimen due to tensile fracture of fibers at the front face (impacted tension side) of the specimen.

The dynamic response of GFRP specimens tested at energy levels 0.1 J – 1.1 J is shown in Fig. 3. The material showed no significant damage up to 0.4 J. As the impact energy increased, a Hertzian failure can be observed at the start of the impact events beyond 0.8 J. The specimens tested at energies between 0.8 J – 1.1 J also exhibited a permanent bending-like deflection after testing (Fig. 3b), which may be due to the visco-elasto-plastic nature of the glass fibres apart from the TPU matrix. The plasticization of matrix played an important role in the resin-rich regions leading to local permanent deformations due to ductility of the TPU matrix. In these non-penetration impact events, the load drops are associated with both elastic and plastic deformations as well as damage initiation. At the higher energy levels, with the increase load, the specimens yielded, implying the onset of plastic deformation represented by the plateau at the top of the curves (Fig. 3b). Thus, the specimens underwent large deformations during loading and, subsequently, a snap-back during the rebound (with the striker slipping past the specimen), represented by the drops and kinks in Figs. 3a and b, respectively. These drops corresponded to the loss of contact between the hammer and the specimen for a short period of time during slippage/snap-back. Unlike the CFRP specimens, the peak loads remained almost the same with appreciable increase in the deformation of GFRP specimens at higher impact energies. It was also observed that the GFRP laminate required higher impact energies for specified damage and failure due to its greater capacity of storing elastic energy.

In the flexural dynamic tests, the energy levels required for the failure of thin laminates were lower than those in traditional drop-weight impact tests. The reason is that in the latter case all the edges of the specimens are usually fully clamped and, thus, higher in-plane membrane stresses and flexural rigidity are developed in thin composite plates. In contrast, in the Izod-type bending tests, with only one side of the specimen clamped and the rest free, membrane stresses is lower. Also, the specimen's thickness is small in comparison with its dimensions resulting in lower flexural rigidity. Obviously, flexural rigidity of the composite specimens depends on material's stiffness, their geometry (size) and boundary conditions.

Further, increasing material's thickness means stiffer and stronger specimens due to their higher flexural rigidity, resulting in higher impact energy for the specified damage initiation and propagation as observed in [5]. Hence, the decrease in flexural rigidity and stress-stiffening effect in the thin cantilevered specimens required lower energy for their deformation, initiation and propagation of damage and ultimate fracture.

In experimental tests of CFRP specimens, the contact duration remained almost the same with increase in the impact velocity (Fig. 2a). Such a response indicates that the material's behaviour is strain rate-independent under dynamic loading in fibre-dominated modes as was also observed in [19]. However, the on-axis GFRP specimens exhibited a rate-dependent behaviour as the contact duration increased with the impact energy (Fig. 3a). The peak loads for CFRP specimens were higher than those of GFRP at the corresponding energy levels due to the higher material's stiffness. The latter also resulted in lower contact duration for CFRP specimens than that for GFRP at the respective impact energy levels. However, GFRP composites did not exhibit a catastrophic fracture like CFRP composites but rather deformed permanently at higher impact energies (Fig. 3b). This means that although GFRP composites are less strong but they sustain higher impact energy before their collapse. It can be delineated from the dynamic tests' results that a required peak force can be obtained by varying impact velocity for a constant hammer mass; while a given impact duration can be obtained by choosing the appropriate material's stiffness. Thus, the qualitative behaviour of GFRP specimens was different to that of CFRP, especially at higher energy levels. In the next sections, the damage behaviour only of CFRP laminates is studied with micro-CT and FE simulations; its choice was based on its higher properties.

### 2.4. Damage Characterization

In this study, X-ray micro-CT measurements of tested CFRP specimens were carried out on XT H 225 X-ray scanner. The system consisted of an X-ray detector and an electronic X-ray source, creating 2D cross-sections of the sample. The source was a sealed X-ray tube operating at 25–225 kV with a 3 μm spot size. Following acquisition of tomographic data for the sample, a software program built a precise 3D map from 2D radiograph images by 'stacking' the individual slices on top of each other; this process is known as *reconstruction*. As denser materials absorb more X-rays than voids and air, this attenuation contrast allows detection and characterisation of cracks and flaws in tomographic images. Two small samples, one with dimensions 8.31 mm x 6.50 mm x 1.0 mm from the impact region and second 7.90 mm x 6.10 mm x

1.0 mm from the fractured region of the CFRP specimen tested at 0.6 J were prepared. Data for the samples was collected at 80 kV and 85 μA. Transmission X-ray images were acquired from 3600 rotation views over 360° of rotation (rotation step of 0.1º) for 3D reconstruction. The obtained data was reconstructed using CT-Pro software, and the analysis of the resulting 3D volumes was performed with the VG Studio Max 2.2 software to partition and highlight regions of interest.

The reconstructed tomographs of the CFRP specimen from the impact location tested at impact energy of 0.6 J are presented in Fig. 4. The images show matrix cracking, delamination and tow debonding at the hammer's impact location along the specimen's height. Dark-grey regions in images represent cracks and damage whereas light-grey areas represent a higher-density material, i.e. carbon-fibre tows. Damage initiation first started below the striker ends at the impact location as represented by dents in the tows in Fig. 4a. The damage then grew within the specimen as the impact force increased with time until the fabric fracture occurred at the cantilever support (vice) at maximum load. At the impact location (Fig. 4c), the interface on the impact side (specimen's front side) is more damaged, which is different to the conical pattern of damage from bottom-to-top in drop weight impact tests studied in [9, 11]. Unlike the drop-weight test conditions, here, the specimen acted as a cantilever beam subjected to large-deflection bending, where the front (top) plies experienced tensile stresses and the back (bottom) ones compressive stresses. The tensile stresses caused more damage on the specimen's impact (front) side than the compressive stresses on the non-impact (back) side. Damage in the middle plies was caused by the maximum interlaminar shear stress at the neutral plane of the specimen. Hence, such a stress distribution was responsible for the front-to-back (top-to-bottom) pattern of damage formation in the specimen. These observations are also corroborated by the stress distribution obtained through numerical analysis described below (see Fig. 13a). All the resin-rich interfaces underwent inter-ply delamination below the impactor. Further, in drop-weight impact specimens, the damage mode is usually dominated by contact and shear stresses causing penetration and perforation at the impact location; whereas, here in the dynamic bending, damage was dominated by a flexural-membrane stress in the tested specimens.

Figure 5 shows the reconstructed 3D images of the CFRP specimen at the bending (fractured) location. Realisation of inter-ply and intra-ply damage mechanisms at its outer edge, 25%, 50%, and 75% of the sample's width is shown in Figs. 5a, b, c, and d, respectively. It was shown that before ultimate fracture, the laminate exhibited matrix cracking and then delaminations and tow debondings near the specimen's

support. Matrix cracks developed in the weak resin-rich pockets around the tows. Inter-ply delamination and intra-ply delamination such as tow debonding can also be observed. These delaminations normally appeared near the matrix cracks regions, which suggested that formation of cracks initiated delamination. In the fibre-rich regions, damage was apparently linked to debonding at the fibre/matrix interface. Such damage is usually caused by the local stress concentrations at the tow/fibre crimps in woven composites under tensile loads. The analysis of internal structure showed that at the time of fabric fracture, which was triggered by tensile fibre failure, almost every ply was delaminated. This delamination is more pronounced in Figs. 5a and c than in 5b and d. The reason is that warp tows, which are aligned along the specimen's axis, bear a higher load than transverse weft tows in bending of the specimen under impact. All the tomographs showed that matrix cracking, delamination and tow debonding were the prominent damage modes at the specimen's impact location, whereas at the bending location, these modes were coupled with fabric fracture.

## 3. Numerical Simulations

The complex weaving architecture as well as multiple modes of damage at various length scales in woven composites makes the micro-mechanics-based constituent-level modelling more computationally expensive for a real-size problem. Thus, a meso-level modelling approach dealing with homogeneous orthotropic plies and a cohesive interface connecting two adjacent plies was adopted to investigate the macro-level response of specimens with dimensions used in tests. Such a meso-level approach coupled with CDM was used in [5, 10, 20] to analyse the damage behaviour of woven composite structures. Here, a discrete modelling approach based on the CZM rather than CDM is employed to realise the out–of-plane fabric fracture apart from the interface delamination and their interaction, without any compromise on the global behaviour of the structure. In the FE models, the material was assumed to have purely elastic orthotropic behavior before the damage initiation. Delamination damage and fabric fracture were assumed to be confined to interfaces, located between the predefined damageable regions, and through-thickness transverse straight cut at the specimen's fracture location, respectively. Both the impactor and the specimen were defined as deformable bodies in the contact interactions to simulate the real-world physics of the problem. A friction coefficient of 0.3 was assumed between the CFRP specimen and the steel hammer as used in [21].

### 3.1. Finite-element model

In this study, three 3D FE models – Models I, II and III as shown in Fig. 6 – were developed to simulate a dynamic behaviour of damaged and fractured CFRP specimens at impacts with energy levels 0.5 J and 0.6 J, respectively. In Model I of the damaged specimen at 0.5 J impact energy; CZEs were defined at the resin-rich interfaces between the laminate's plies. Hence, Model I contained three longitudinal cohesive layers - one in front of the beam's neutral plane (NP), the second coinciding with it, and the third to the back of the NP to simulate multiple delamination scenarios. Model II is similar to Model I except the top edge of the specimen is fully constrained to create the conditions of fixed-fixed specimen (quasi drop weight test simulation) under dynamic bending. Model II was developed to investigate the effect of boundary conditions on the damage evolution under dynamic loading. Model III (fractured specimen at 0.6 J) had, in addition to the same three interface layers of CZEs, one more through-thickness transverse cohesive layer placed at the specimen's fracture location, to model both the inter-ply delamination and intra-ply fabric fracture and their interaction. The following notation is used for cohesive layers in Models I, II and III: FCL - in front of the NP (towards impact face), MCL - the cohesive layer coinciding with the NP, and BCL - the one to the back of the NP; the through-thickness transverse layer is denoted as CCL. These cohesive layers were included in the model since the location of damage initiation is *a priori* known from the micro-CT analysis in this study. However, the location of damage initiation within a composite laminate can also be described analytically. Particularly, cohesive elements can be placed at interfaces between plies having different orientations, which are more prone to inter-ply delamination [14]. In addition, they can also be placed in matrix-dominated regions such as interfaces between the layers with the same orientation, especially at the mid-plane of the laminate, which are more susceptible to damage initiation due to their low interlaminar shear strength [5]. However, increasing the number of cohesive layers will increase the computational cost and the solution convergence may become rather complicated [13]. Since CFRP composites are essentially strain rate-independent in fibre-dominated modes such as on-axis $[0°,90°]_{2s}$ laminates subjected to in-plane tension and compression in the low-velocity (low strain-rate) regimes, the material constants obtained from the quasi-static tests (Table 2) were used in the FE models. Similarly, the cohesive law was assumed to be strain-rate insensitive, and thus static fracture-toughness values were assumed for a dynamic crack growth; this was proven to be sufficient in previous dynamic-fracture studies [22].

Cohesive-zone elements (CZEs) were used to model both the inter-ply and intra-ply damage modes and their interaction in CFRP laminates. The nominal quadratic stress criterion was used for damage initiation, whereas the Benzeggagh and Kenane criterion [23] was used for damage propagation. Parameters of the cohesive-zone elements presented in Table 3 were taken from the authors' previous work [17]. Apart from inter-ply damage modelling, CZEs have also been used to model intra-ply damage mechanisms such as splitting and ply fracture in composite laminates [16]. Here, the initiation of intra-ply fabric damage was linked to average ultimate flexural strength of 720 MPa in both warp and weft directions from the quasi-static bending tests. Intra-ply fracture evolution was based on fabric fracture energy of 40 kJ/m$^2$ in both warp and weft directions as reported in [10] for a similar carbon fabric. The stiffness of finite-thickness cohesive elements was calibrated according to $K = E_{33}/t_i$, proposed by Daudeville *et al.* [24], where $E_{33}$ (8 GPa) is the material's through-thickness stiffness and $t_i$ - 16 µm (taken from [25]) is the thickness of resin-rich interface between plies; resulting in interface stiffness of 5 x 10$^{14}$ N/m$^3$ for inter-ply damage. However, stiffness of the interface elements defined for intra-ply fracture was based on the longitudinal elastic stiffness $E_{11}$ of the ply instead of $E_{33}$ in the above relation resulting in a higher value of 1x10$^{15}$ N/m$^3$. Further details of the FE modelling such as the modelled test set-up, geometry, mesh and element types, and boundary conditions can be seen elsewhere [25].

### 3.2. Discussion of simulations results

#### 3.2.1. Response of damaged specimen

Comparison of the experimental and predicted force-time responses and evolution of damage at the impact location of of CFRP laminate in FE Model I at impact energy of 0.5 J is shown in Fig. 7. Fluctuations in the experimental force-time history designated as $F_d$ - Exp representing the internal damage initiation (load drops in Fig. 7) are observed before the peak load is reached. Apparently, both the global response and the contact duration are reasonably well predicted for the damaged specimen. However, the numerical damage threshold $F_d$ - FE, at which a significant change in the laminate stiffness was detected, was under-predicted in the FE model. This discrepancy might be due to the meso-level formulation for the plies in the model. Apparently, in experiments, the fabric-reinforced laminates absorbed more energy due to the ductile resin-rich pockets and the interlacing of fibres in two orthogonal directions, and, thus, offered more resistance to damage initiation, which were not taken into account in the simulations. However, in Fig. 7, the impact force and duration in numerical simulations are higher

than those in experiments, asserting higher energy dissipation in the FE model. This extra energy could be caused by an exaggerated amount of viscous dissipation in the model after damage initiation.

Similarly, the evolution of damage area at the impact location calculated with Model I is also plotted in Fig. 7. Figure 8 shows the calculated delamination area at three interfaces – FCL, MCL and BCL – in simulation with Model I at two different time intervals: at 3 ms (after $F_d$ - FE; Fig. 7) and at 6 ms (near peak load; Fig. 7). Here, delamination initiated first at the point of striker impact and then at the bending location of the cantilevered CFRP specimen. The ends of the trace were damaged more due to sharp corners of the hammer striker. A large and quick increase in the delamination area was observed simultaneously in all the layers beyond the time corresponding to $F_d$ - FE. It can be seen from both Figs. 7 and 8 that the largest area of delamination occurred at the mid-plane interface layer MCL due to the high level of through-thickness shear stress. Thus, a Mode-II type delamination initiated in the specimen's mid-region, where shear stress reached the interface shear strength, and grew more in MCL than FCL and BCL at the impact location. Similarly, the maximum bending stresses at the upper (front) and lower (back) plies were foremost responsible for damage formation at FCL and BCL of the specimen, especially at the bending location (Fig. 8). After the load peak was reached at 6 ms, the damage growth stopped in the unloading region of the load-time response (Fig. 7). The size and shape of the individual delaminations could not be compared to their experimental counterparts as such experimental results were not possible with the micro-CT for the full-scale specimen due to the requirement of field of view of the system. Also, due to the weaving architecture of the laminate, the spread of the damage is not in a 2D plane. Here, the in-situ quantification of various damage modes is either very cumbersome or non-feasible.

The main focus of the FE study is to compare and analyse the salient features of the dynamics and damage evolution in flexural (cantilevered) and quasi drop weight tests (two ends fixed) specimens. The load history and evolution of damage with time for Model II, where the specimen was constrained as a fixed-fixed beam, is presented in Fig. 9. The fixed-fixed boundary conditions increased the flexural rigidity of thin laminates resulting in a high peak of the impact force - 600 N, which is approximately 7.5 times more than that predicted with only one end fixed (cantilevered) specimen (see Fig. 7). The impact duration also reduced from 12 ms to 2.5 ms due to increased stiffness of the fixed-fixed specimen. Figure 10 shows the extent of delamination area at three interfaces – FCL, MCL and BCL – in simulations with Model II for fixed-fixed specimen at two different time intervals: at 0.2 ms (just at $F_d$ - FE; Fig. 9) and at

1.2 ms (near peak load; Fig. 9). Here, the damage pattern is also different due to the constraints. Due to the higher impact force, the extent and magnitude of damage at the impact location are higher especially near the constrained top edge than that shown in Fig. 8. Here, too, the MCL is more damaged at the impact location.

To investigate the effect of constraints on inter-ply damage evolution, comparison of damage progression in both Models I and II with cantilevered and both ends fixed (quasi drop weight, qDW) conditions, respectively, is presented in Fig. 11. The rate of damage growth in quasi drop weight specimen is faster than that of cantilevered one. This demonstrates that due to both ends fixed, the specimen of the same size under similar impact energy of 0.5 J dissipates a lot of energy very quickly than the cantilevered specimen in Model I. Further, the extent of damage is also higher in quasi drop weight model in all interface layers than that of cantilevered specimen. Here, it can be inferred from these results that the boundary conditions of the specimens has not only a significant effect on the impact force and duration but also on the damage evolution within the specimen.

**3.3.2. Response of fractured specimen**

Fabric fracture occurred as the impact energy was increased to 0.6 J in experimental tests. The predicted evolution of impact force in Model III is compared with experimental results at this level of energy in Fig. 12. Here, too, the load drops designated as $F_d$ - Exp and $F_d$ - FE represents delamination initiation for the experiments and numerical results, respectively. The experimental curve shows more fluctuations due to significant damage after the damage threshold $F_d$ - Exp at higher impact energy, followed by the ultimate ply fracture at 4.8 ms. The final ply fracture is presented by a sudden drop in the impact force; however, the load didn't drop to zero, because in dynamic bending the distal plies in compression were not fractured causing a residual load of about 22 N. The simulation showed the ply fracture somewhat earlier - at 4.38 ms, which might be due to the low ply fracture initiation strength defined in Model III. Still, the FE analysis gave a good prediction of the important characteristics of the failure process.

The sequence of inter-ply delamination and intra-ply fabric breakage as well as their interaction in Model III is illustrated in the deformed contour plots for flexural stress $\sigma_{11}$ shown in Fig. 13. Although the laminate was fully delaminated in Fig. 13a, the flexural stress contours were almost uniform. The stress reduced as the first ply's fracture occurred at 4.38 ms as shown in Fig. 13b followed by fracture of the second ply in Figs. 13c at 4.62 ms. The third and fourth plies remained intact because of compressive

stresses on back side of the specimen in the bending. These plies carried the residual load and were in tension and compression states, respectively, as can be seen in Figs. 13c and d. Stress concentration at the locations of inter-ply and intra-ply crack tips is apparent in Figs. 13b-d. As the load increased, the ply elements moved relative to each other as in Mode-II type fracture along the delaminated interface layers as shown in Fig. 13d. There may be the possibility of fibre kinking due to buckling instability in the back plies under compression; however, this behaviour is not studied in the meso-scale models.

## 4. Conclusions

The behaviour of fabric-reinforced composites under dynamic bending was studied using experimental tests, micro-CT scanning and numerical simulations. The dynamic tests revealed that the CFRP laminates were fractured at lower energy levels than GFRP due to their lower energy absorbing capability. However, the impact strength of the CFRP laminates was higher than that of GFRP. Further, on-axis GFRP laminates exhibited a strain-rate sensitive behaviour as compared to CFRP specimens. In the impact bending tests, the specimens failed at lower impact energy as compared to their failure in drop weight impact tests. It was also found that damage in the specimens at the impact location was from its front to the back in the large-deflection impact tests, unlike the bottom-to-top character in drop weight tests. Considerable matrix cracking leading to tow debonding and delamination was observed along with tow fibre fracture in the micro-CT scanning of the impacted CFRP laminates. This microstructural characterisation formed a basis for damage incorporation in the developed 3D FE models.

The results of meso-scale 3D FE models of CFRP laminates were close to the experimental ones, and, the simulations were capable to reproduce the damage sequence and patterns observed experimentally. The numerical models helped to offer significant information about the complex damage phenomena that occurred at various stages of impact bending. For instance, interaction of delamination and ply fracture, which cannot be assessed directly in real tests and by non-destructive investigation, was captured with the CZM-based modelling approach. Similarly, the effect of boundary conditions on the dynamic response was also predicted for the first time, which is hard to obtain experimentally for the fixed-fixed conditions. Such conditions resulted in an increased flexural rigidity of the impacted specimen and the higher peak load and reduced impact duration. These quasi drop weight test conditions also resulted in a larger extent of damage with a faster growth rate. This also corroborated our observations that cantilever specimens failed at lower impact energies than fully clamped specimens in drop weight impact tests.

**References**

[1] Sutcliffe MPF, Monroy Aceves C, Stronge WJ, Choudhry RS, Scott AE. Moderate speed impact damage to 2D-braided glass–carbon composites. Composite Structures. 2012;94(5):1781-1792.

[2] Naik N, Chandra Sekher Y, Meduri S. Damage in woven-fabric composites subjected to low-velocity impact. Composites Science and Technology. 2000;60(5):731-744.

[3] Crabtree P, Dhokia V, Newman S, Ansell M. Manufacturing methodology for personalised symptom-specific sports insoles. Robotics and Computer-Integrated Manufacturing. 2009;25(6):972-979.

[4] http://www.ossur.com. 2013.

[5] Menna C, Asprone D, Caprino G, Lopresto V, Prota A. Numerical simulation of impact tests on GFRP composite laminates. International Journal of Impact Engineering. 2011;38(8–9):677-685.

[6] Scott A, Mavrogordato M, Wright P, Sinclair I, Spearing S. In situ fibre fracture measurement in carbon–epoxy laminates using high resolution computed tomography. Composites Science and Technology. 2011;71(12):1471-1477.

[7] Sket F, Seltzer R, Molina-Aldareguía J, Gonzalez C, LLorca J. Determination of damage micromechanisms and fracture resistance of glass fiber/epoxy cross-ply laminate by means of X-ray computed microtomography. Composites Science and Technology. 2012;72:350-359.

[8] Ullah H, Harland A, Silberschmidt V. Experimental and Numerical Analysis of Damage in Woven GFRP Composites Under Large-deflection Bending. Applied Composite Materials. 2012;19(5):769-783.

[9] Aktaş M, Ersen Balcıoğlu H, Aktaş A, Türker E, Emin Deniz M. Impact and post impact behavior of layer fabric composites. Composite Structures. 2012;94:2809-2818.

[10] Iannucci L, Willows M. An energy based damage mechanics approach to modelling impact onto woven composite materials--Part I: Numerical models. Composites Part A: Applied Science and Manufacturing. 2006;37(11):2041-2056.

[11] Kim JK, Sham ML. Impact and delamination failure of woven-fabric composites. Composites Science and Technology. 2000;60(5):745-761.

[12] Wisnom MR, Hallett SR. The role of delamination in strength, failure mechanism and hole size effect in open hole tensile tests on quasi-isotropic laminates. Composites Part A. 2009;40(4):335-342.

[13] Ullah H, Harland AR, Lucas T, Price D, Silberschmidt VV. Finite-element modelling of bending of CFRP laminates: Multiple delaminations. Computational Materials Science. 2012;52(1):147-156.

[14] Wisnom MR. Modelling discrete failures in composites with interface elements. Composites Part A. 2010;41(7):795-805.

[15] Fang XJ, Zhou ZQ, Cox BN, Yang QD. High-fidelity simulations of multiple fracture processes in a laminated composite in tension. Journal of the Mechanics and Physics of Solids. 2011;59(7):1355-1373.

[16] Hallett SR, Jiang WG, Khan B, Wisnom MR. Modelling the interaction between matrix cracks and delamination damage in scaled quasi-isotropic specimens. Composites Science and Technology. 2008;68(1):80-89.

[17] Ullah H, Harland AR, Silberschmidt VV. Damage modelling in woven-fabric CFRP laminates under large-deflection bending. Computational Materials Science. 2012;64:130-135.

[18] Hosur M, Adbullah M, Jeelani S. Studies on the low-velocity impact response of woven hybrid composites. Composite Structures. 2005;67(3):253-262.

[19] López-Puente J, Li S. Analysis of strain rate sensitivity of carbon/epoxy woven composites. International Journal of Impact Engineering. 2012;48(0):54-64.

[20] Sokolinsky VS, Indermuehle KC, Hurtado JA. Numerical simulation of the crushing process of a corrugated composite plate. Composites Part A: Applied Science and Manufacturing. 2011;42:1119-1126.

[21] Lopes C, Camanho P, Gürdal Z, Maimí P, González E. Low-velocity impact damage on dispersed stacking sequence laminates. Part II: Numerical simulations. Composites Science and Technology. 2009;69(7-8):937-947.

[22] Gözlüklü B, Coker D. Modeling of the dynamic delamination of L-shaped unidirectional laminated composites. Composite Structures. 2012;94(4):1430-1442.

[23] Benzeggagh ML, Kenane M. Measurement of mixed-mode delamination fracture toughness of unidirectional glass/epoxy composites with mixed-mode bending apparatus. Composites Science and Technology. 1996;56(4):439-449.

[24] Daudeville L, Allix O, Ladeveze P. Delamination analysis by damage mechanics: some applications. Composites Engineering. 1995;5(1):17-24.

[25] Ullah H, Harland AR, Silberschmidt VV. Damage and fracture in carbon fabric reinforced composites under impact bending. Composite Structures. 2013;101(0):144-156.

**Figure Captions**

Fig. 1. Resil impact test set-up

Fig. 2. Experimental response of twill 2/2 CFRP laminates at various impact energies: (a) force-time curves; (b) force-deflection curves

Fig. 3. Experimental response of twill 2/2 GFRP laminates at various impact energies: (a) force-time curves; (b) force-deflection curves

Fig. 4. Reconstructed 3D tomographs of twill 2/2 CFRP specimen at impact location across height of sample (resolution 6.7 μm): (a) edge; (b) 25% (1 mm above impact centre line) (c) 50% (at impact centre); (d) 75% (below impact centre line) of height

Fig. 5. Reconstructed 3D tomographs of twill 2/2 CFRP specimen at bending (fracture) location across width of sample (resolution 6.1 μm): (a) edge; (b) 25%; (c) 50%; (d) 75% of width

Fig. 6. Schematics of FE models for cantilever bending (Model I) (a), fixed-fixed bending ( quasi drop weight test simulation) (Model II) (b) and fractured (Model III) (c) behaviours of CFRP specimens tested at 0.5 J and 0.6 J impact energy, respectively

Fig. 7. Comparison of experimental and numerical force-time response and evolution of inter-ply delamination area at the impact location of CFRP laminate in FE Model I at impact energy of 0.5 J

Fig. 8. Delamination evolution in FE Model I at impact energy of 0.5 J at 3 ms (a) and 6 ms (b) [25]

Fig. 9. Numerical force-time response and damage evolution in FE Model II with fixed-fixed boundary (quasi drop weight (qDW) test) conditions at impact energy of 0.5 J

Fig. 10. Delamination evolution in FE Model II with fixed-fixed boundary conditions of the specimen at impact energy of 0.5 J at 0.2 ms (a) and 1.2 ms (b)

Fig. 11. Comparison of damage evolution under cantilever (flexural) and fixed-fixed (qDW) conditions of CFRP laminates from FE Models I and II at 0.5 J impact energy, respectively

Fig. 12. Comparison of experimental and numerical (Model III) force-time response for CFRP laminates at impact energy of 0.6 J

Fig. 13. Contours of bending stress $\sigma_{11}$ in Model III showing interaction of inter-ply and intra-ply damage at impact energy of 0.6 J at 4.2 ms (a), 4.38 ms (b), 4.62 ms (c) and 6.0 ms (d) (side view; scaling factor 0.5; fractured interfaces are represented by white colour)

**Table captions**

Table 1. Parameters of twill 2/2 woven composites

Table 2. Material properties of twill 2/2 woven composites

Table 3. Material parameters of inter-ply cohesive elements

# Evolution and interaction of damage modes in fabric-reinforced composites under dynamic flexural loading

HIMAYAT ULLAH, ANDY. R. HARLAND, VADIM.V. SILBERSCHMIDT*

*Wolfson School of Mechanical and Manufacturing Engineering, Loughborough University, Leicestershire, LE11 3TU, UK*

* Corresponding author: Ashby Road, Loughborough, Leics., LE11 3TU, UK.

Phone: +44 1509 227504. Fax: +44 1509 227502, E-mail: V.Silberschmidt@lboro.ac.uk

**Abstract**

In this paper, an experimental study is performed to characterise the behaviour of fabric-reinforced composites used in sports products under large-deflection bending in Izod-type impact tests. X-ray micro computed tomography (micro-CT) is used to investigate various damage modes in the impacted CFRP specimens. It revealed that matrix cracking, delaminations, tow debonding, and fibre fracture were the prominent damage modes. Three-dimensional finite-element models are developed to study the onset, progression and interaction of some damage modes such as delamination and fabric fracture observed with micro-CT. A damage modelling technique based on a cohesive-zone method, which is more efficient than continuum damage mechanics approach, is proposed for analysis of interaction of damage modes. The developed numerical models are capable to simulate the damage mechanisms and their interaction observed in the tests. In this study, the pattern of damage formation observed in specimens was front-to-back, unlike bottom-to-top one in drop weight impact tests. The effect of boundary conditions on the dynamic response and damage evolution of composite laminates is also investigated.

Keywords: A. Fabric, B. Impact behaviour, B. Delamination, B. Fracture, C. Modelling

## 1. Introduction

The application of woven composites such as carbon fabric-reinforced polymer (CFRP) and glass fabric-reinforced polymer (GFRP) laminates is ever increasing in impact-prone structures due to their better resistance to impact damage particularly delamination and fracture toughness than unidirectional tape laminates [1, 2]. Apart from aerospace and automotive structural elements, woven composites are also incorporated in design of sports products that could be subjected to large-deflection bending caused by dynamic loading. Composite structures such as aircraft wings, automotive bumpers and sports products e.g. athletic footwear insoles [3] and a custom-built Flex-Foot Cheetah blade for elite amputee athletes [4]

are subjected to large-deflection bending caused by low-velocity impacts during service. In contrast to traditional impact events such as bird strike or tool drop, kinematics, velocity and energy of large-deflection dynamic bending events are significantly different which cannot be replicated by drop weight testing where the flexure is significantly constrained; hence, should be properly studied. The damage mechanisms typically caused by impact loads in composite structures are matrix cracking, fibre breakage, delamination between adjacent layers and, ultimately, fabric fracture [5]. These damage modes are usually investigated with the use of 2D damage characterization techniques such as visual inspection, microscopy, radiography and ultrasonography, which are not adequate for analysis of inherently 3D damage processes within the composite laminates. Further, these conventional techniques are either destructive or do not provide a reasonable spatial resolution. These shortcomings can be alleviated with the application of non-destructive X-ray micro-CT technique, which can provide 3D images of internal realisation of damage mechanisms and their interaction in the composites with high resolution. This relatively recent technique has been used to investigate damage mechanisms in composites at micron scale [6-8]. Therefore, in this study, damage suffered by the composites under new types of loading regimes such as large-deflection dynamic bending experienced by various products in service was investigated using micro-CT.

The behaviour of fabric-reinforced composites subjected to low-velocity impact was widely studied in [2, 9-11] among others. However, majority of the work deals with the behaviour of composites studied with drop weight impact tests, usually causing penetration and perforation damage in impacted laminates in which flexure is significantly constrained. A large-deflection dynamic bending behaviour of composite structures which can be replicated by a pendulum-type impactor is rarely investigated. Further, the inter-ply delamination is usually analysed with cohesive-zone models (CZMs) [12, 13], whereas the intra-ply damage mechanisms are normally predicted using continuum damage mechanics (CDM) [5, 10]. As observed in recent studies, due to the homogenisation process in CDM models, key information on the coupling of multiple damage modes is lost at the macroscopic scale, resulting in inaccurate prediction of a crack path [14]. Advanced CZMs have the potential to couple directly the intra-ply and inter-ply cracks to achieve unification of crack initiation and propagation within a single approach. This damage-interaction modelling approach was adopted in [15, 16] by using cohesive-zone elements (CZEs) in numerical analysis of composite specimens' fracture in tension. This technique was also employed in [8, 17] to

simulate the damage interaction in fabric-reinforced composites subjected to large-deflection quasi-static bending. However, applications of the modelling approach for interacting damage modes to simulate the behaviour of woven composites subjected to dynamic bending are still limited.

In this work, the flexural behaviour of woven CFRP and GFRP laminates subjected to pendulum-type impacts is studied for various levels of impact energy. The development of predictive models for impact behaviour of composites depends on the qualitative assessment of damage modes within the material. For this purpose, micro-structural examination of tested CFRP laminates with the micro-CT technique identified location and type of inter- and intra-ply damage modes. Since multiple modes of damage were observed in CT images, this work addresses modelling of initiation, propagation and interaction of only two major modes - delamination and fabric fracture - in CFRP laminates under dynamic bending. Three-dimensional (3D) FE models were developed in Abaqus/Explicit for specimens damaged and fractured at various impact-energy levels by inserting CZEs at the identified crack locations. In this paper, analysis of large-deflection dynamic bending, CZM-based modelling of damage interaction and comparison of damage evolution in large-deflection bending and constrained bending like quasi drop weight test conditions are the main novel elements of the approach developed to study dynamic damage.

## 2. Experimental methods

### 2.1 Materials

The composites studied were laminates with two different types of fabrics made of carbon and glass fibres reinforcing thermoplastic polyurethane (TPU) matrix. The laminates were produced from 0°/90° prepregs in the form of four plies designated as $[0°,90°]_{2s}$, where 0° and 90° represent yarns in the warp and weft directions, respectively. The laminates had a 2/2 twill balanced and symmetric weaving pattern with a fibre volume fraction of 45%. As damage is sensitive to geometrical parameters of woven laminates such as the size and location of tows and resin within the laminate, thus, main parameters of the laminate and its constituents can be found in Table 1. The elastic constants of CFRP and GFRP determined from the quasi-static tests are presented in Table 2; details of the tests for characterisation of both types of materials are presented elsewhere [8, 17].

### 2.2 Dynamic testing

Dynamic bending tests in a low-velocity range from 1.5 m/s to 2 m/s were carried out according to the ASTM D 4812 standard using an instrumented pendulum-type CEAST Resil impactor as shown in Fig. 1.

Un-notched rectangular specimens of 40 mm length, 25 mm width and 1.0 mm thickness were prepared from CFRP and GFRP laminates. In the dynamic tests, the bottom of the cantilever-like specimen was fixed rigidly in the machine vice; whereas its upper 30 mm part was hit with striker of the pendulum hammer with a controlled level of initial energy, resulting in large-deflection bending of the specimen. The line of contact (impact) of the hammer's striking nose was kept away at a distance of 22 mm from the specimen's fixed support according to the standard (see Fig. 6a). A calibrated impact hammer with a mass of 0.6746 kg and a length of 0.3268 m was employed in this work. Impact tests were performed on CFRP and GFRP specimens at energy levels of 0.1 J – 0.6 J and 0.1 J – 1.1 J, respectively, to determine the fracture energy of the specimens. The impact-force signal was captured by a piezoelectric force transducer fixed to the hammer's striking nose. The signal was registered with a sampling frequency of 227 kHz, with up to 5000 data points recorded per impact test by the data acquisition system DAS 8000 connected to the Resil impact tester.

### 2.3 Discussion of experimental results

Typical transient response of CFRP specimens tested at six different energy levels is presented in Fig. 2. From these plots, it is clear that the slope and the peak load of the force-time (Fig. 2a) and force-deflection (Fig. 2b) curves increased with increase in the impact energy. The slope of force-deflection curves represents the contact stiffness, while the enclosed area under the curves gives the absorbed energy. The descending sections of the curves, where both the load and deflection decrease, represent rebounding of the hammer. Clearly, the area under the curves increased with impact energy indicating an increase in the energy absorbed by CFRP laminates. Energy absorption in composites is mainly through elastic strain energy, plastic deformation and formation of various damage modes [18]. In the materials under study, the TPU matrix material is highly compliant and usually absorbs more energy without causing any appreciable damage. At low energy levels, a linear increase of force with time is observed at the start of loading, representing a purely elastic undamaged response of the specimen. The loading and unloading portions of the force-time curves have a nearly symmetric parabolic shape up to 0.4 J (Fig. 2a), indicating that very little damage has occurred. As the impact energy was increased to 0.5 J, fluctuations in the force-time and force-deflection response could be observed before the peak load was reached. Such fluctuations associated with load drops are caused by internal initiation of damage such as delamination at low incident energy with an associated reduction in the specimen's stiffness [9]. As the load continued

increasing, the damage grew and multiple delaminations at different ply interfaces could occur. The force-time curve became unsymmetrical at 0.5 J with regard to its peak as can be seen in Fig. 2a. The dynamic curves showed more oscillations due to significant damage before the fabric fracture occurred at a higher impact energy of 0.6 J. In Fig. 2a, the fabric rupture is represented by a quick drop in impact force implying a momentary loss of contact between the hammer and specimen due to tensile fracture of fibers at the front face (impacted tension side) of the specimen.

The dynamic response of GFRP specimens tested at energy levels 0.1 J – 1.1 J is shown in Fig. 3. The material showed no significant damage up to 0.4 J. As the impact energy increased, a Hertzian failure can be observed at the start of the impact events beyond 0.8 J. The specimens tested at energies between 0.8 J – 1.1 J also exhibited a permanent bending-like deflection after testing (Fig. 3b), which may be due to the visco-elasto-plastic nature of the glass fibres apart from the TPU matrix. The plasticization of matrix played an important role in the resin-rich regions leading to local permanent deformations due to ductility of the TPU matrix. In these non-penetration impact events, the load drops are associated with both elastic and plastic deformations as well as damage initiation. At the higher energy levels, with the increase load, the specimens yielded, implying the onset of plastic deformation represented by the plateau at the top of the curves (Fig. 3b). Thus, the specimens underwent large deformations during loading and, subsequently, a snap-back during the rebound (with the striker slipping past the specimen), represented by the drops and kinks in Figs. 3a and b, respectively. These drops corresponded to the loss of contact between the hammer and the specimen for a short period of time during slippage/snap-back. Unlike the CFRP specimens, the peak loads remained almost the same with appreciable increase in the deformation of GFRP specimens at higher impact energies. It was also observed that the GFRP laminate required higher impact energies for specified damage and failure due to its greater capacity of storing elastic energy.

In the flexural dynamic tests, the energy levels required for the failure of thin laminates were lower than those in traditional drop-weight impact tests. The reason is that in the latter case all the edges of the specimens are usually fully clamped and, thus, higher in-plane membrane stresses and flexural rigidity are developed in thin composite plates. In contrast, in the Izod-type bending tests, with only one side of the specimen clamped and the rest free, membrane stresses is lower. Also, the specimen's thickness is small in comparison with its dimensions resulting in lower flexural rigidity. Obviously, flexural rigidity of the composite specimens depends on material's stiffness, their geometry (size) and boundary conditions.

Further, increasing material's thickness means stiffer and stronger specimens due to their higher flexural rigidity, resulting in higher impact energy for the specified damage initiation and propagation as observed in [5]. Hence, the decrease in flexural rigidity and stress-stiffening effect in the thin cantilevered specimens required lower energy for their deformation, initiation and propagation of damage and ultimate fracture.

In experimental tests of CFRP specimens, the contact duration remained almost the same with increase in the impact velocity (Fig. 2a). Such a response indicates that the material's behaviour is strain rate-independent under dynamic loading in fibre-dominated modes as was also observed in [19]. However, the on-axis GFRP specimens exhibited a rate-dependent behaviour as the contact duration increased with the impact energy (Fig. 3a). The peak loads for CFRP specimens were higher than those of GFRP at the corresponding energy levels due to the higher material's stiffness. The latter also resulted in lower contact duration for CFRP specimens than that for GFRP at the respective impact energy levels. However, GFRP composites did not exhibit a catastrophic fracture like CFRP composites but rather deformed permanently at higher impact energies (Fig. 3b). This means that although GFRP composites are less strong but they sustain higher impact energy before their collapse. It can be delineated from the dynamic tests' results that a required peak force can be obtained by varying impact velocity for a constant hammer mass; while a given impact duration can be obtained by choosing the appropriate material's stiffness. Thus, the qualitative behaviour of GFRP specimens was different to that of CFRP, especially at higher energy levels. In the next sections, the damage behaviour only of CFRP laminates is studied with micro-CT and FE simulations; its choice was based on its higher properties.

### 2.4. Damage Characterization

In this study, X-ray micro-CT measurements of tested CFRP specimens were carried out on XT H 225 X-ray scanner. The system consisted of an X-ray detector and an electronic X-ray source, creating 2D cross-sections of the sample. The source was a sealed X-ray tube operating at 25–225 kV with a 3 μm spot size. Following acquisition of tomographic data for the sample, a software program built a precise 3D map from 2D radiograph images by 'stacking' the individual slices on top of each other; this process is known as *reconstruction*. As denser materials absorb more X-rays than voids and air, this attenuation contrast allows detection and characterisation of cracks and flaws in tomographic images. Two small samples, one with dimensions 8.31 mm x 6.50 mm x 1.0 mm from the impact region and second 7.90 mm x 6.10 mm x

1.0 mm from the fractured region of the CFRP specimen tested at 0.6 J were prepared. Data for the samples was collected at 80 kV and 85 µA. Transmission X-ray images were acquired from 3600 rotation views over 360° of rotation (rotation step of 0.1º) for 3D reconstruction. The obtained data was reconstructed using CT-Pro software, and the analysis of the resulting 3D volumes was performed with the VG Studio Max 2.2 software to partition and highlight regions of interest.

The reconstructed tomographs of the CFRP specimen from the impact location tested at impact energy of 0.6 J are presented in Fig. 4. The images show matrix cracking, delamination and tow debonding at the hammer's impact location along the specimen's height. Dark-grey regions in images represent cracks and damage whereas light-grey areas represent a higher-density material, i.e. carbon-fibre tows. Damage initiation first started below the striker ends at the impact location as represented by dents in the tows in Fig. 4a. The damage then grew within the specimen as the impact force increased with time until the fabric fracture occurred at the cantilever support (vice) at maximum load. At the impact location (Fig. 4c), the interface on the impact side (specimen's front side) is more damaged, which is different to the conical pattern of damage from bottom-to-top in drop weight impact tests studied in [9, 11]. Unlike the drop-weight test conditions, here, the specimen acted as a cantilever beam subjected to large-deflection bending, where the front (top) plies experienced tensile stresses and the back (bottom) ones compressive stresses. The tensile stresses caused more damage on the specimen's impact (front) side than the compressive stresses on the non-impact (back) side. Damage in the middle plies was caused by the maximum interlaminar shear stress at the neutral plane of the specimen. Hence, such a stress distribution was responsible for the front-to-back (top-to-bottom) pattern of damage formation in the specimen. These observations are also corroborated by the stress distribution obtained through numerical analysis described below (see Fig. 13a). All the resin-rich interfaces underwent inter-ply delamination below the impactor. Further, in drop-weight impact specimens, the damage mode is usually dominated by contact and shear stresses causing penetration and perforation at the impact location; whereas, here in the dynamic bending, damage was dominated by a flexural-membrane stress in the tested specimens.

Figure 5 shows the reconstructed 3D images of the CFRP specimen at the bending (fractured) location. Realisation of inter-ply and intra-ply damage mechanisms at its outer edge, 25%, 50%, and 75% of the sample's width is shown in Figs. 5a, b, c, and d, respectively. It was shown that before ultimate fracture, the laminate exhibited matrix cracking and then delaminations and tow debondings near the specimen's

support. Matrix cracks developed in the weak resin-rich pockets around the tows. Inter-ply delamination and intra-ply delamination such as tow debonding can also be observed. These delaminations normally appeared near the matrix cracks regions, which suggested that formation of cracks initiated delamination. In the fibre-rich regions, damage was apparently linked to debonding at the fibre/matrix interface. Such damage is usually caused by the local stress concentrations at the tow/fibre crimps in woven composites under tensile loads. The analysis of internal structure showed that at the time of fabric fracture, which was triggered by tensile fibre failure, almost every ply was delaminated. This delamination is more pronounced in Figs. 5a and c than in 5b and d. The reason is that warp tows, which are aligned along the specimen's axis, bear a higher load than transverse weft tows in bending of the specimen under impact. All the tomographs showed that matrix cracking, delamination and tow debonding were the prominent damage modes at the specimen's impact location, whereas at the bending location, these modes were coupled with fabric fracture.

## 3. Numerical Simulations

The complex weaving architecture as well as multiple modes of damage at various length scales in woven composites makes the micro-mechanics-based constituent-level modelling more computationally expensive for a real-size problem. Thus, a meso-level modelling approach dealing with homogeneous orthotropic plies and a cohesive interface connecting two adjacent plies was adopted to investigate the macro-level response of specimens with dimensions used in tests. Such a meso-level approach coupled with CDM was used in [5, 10, 20] to analyse the damage behaviour of woven composite structures. Here, a discrete modelling approach based on the CZM rather than CDM is employed to realise the out–of-plane fabric fracture apart from the interface delamination and their interaction, without any compromise on the global behaviour of the structure. In the FE models, the material was assumed to have purely elastic orthotropic behavior before the damage initiation. Delamination damage and fabric fracture were assumed to be confined to interfaces, located between the predefined damageable regions, and through-thickness transverse straight cut at the specimen's fracture location, respectively. Both the impactor and the specimen were defined as deformable bodies in the contact interactions to simulate the real-world physics of the problem. A friction coefficient of 0.3 was assumed between the CFRP specimen and the steel hammer as used in [21].

### 3.1. Finite-element model

In this study, three 3D FE models – Models I, II and III as shown in Fig. 6 – were developed to simulate a dynamic behaviour of damaged and fractured CFRP specimens at impacts with energy levels 0.5 J and 0.6 J, respectively. In Model I of the damaged specimen at 0.5 J impact energy; CZEs were defined at the resin-rich interfaces between the laminate's plies. Hence, Model I contained three longitudinal cohesive layers - one in front of the beam's neutral plane (NP), the second coinciding with it, and the third to the back of the NP to simulate multiple delamination scenarios. Model II is similar to Model I except the top edge of the specimen is fully constrained to create the conditions of fixed-fixed specimen (quasi drop weight test simulation) under dynamic bending. Model II was developed to investigate the effect of boundary conditions on the damage evolution under dynamic loading. Model III (fractured specimen at 0.6 J) had, in addition to the same three interface layers of CZEs, one more through-thickness transverse cohesive layer placed at the specimen's fracture location, to model both the inter-ply delamination and intra-ply fabric fracture and their interaction. The following notation is used for cohesive layers in Models I, II and III: FCL - in front of the NP (towards impact face), MCL - the cohesive layer coinciding with the NP, and BCL - the one to the back of the NP; the through-thickness transverse layer is denoted as CCL. These cohesive layers were included in the model since the location of damage initiation is *a priori* known from the micro-CT analysis in this study. However, the location of damage initiation within a composite laminate can also be described analytically. Particularly, cohesive elements can be placed at interfaces between plies having different orientations, which are more prone to inter-ply delamination [14]. In addition, they can also be placed in matrix-dominated regions such as interfaces between the layers with the same orientation, especially at the mid-plane of the laminate, which are more susceptible to damage initiation due to their low interlaminar shear strength [5]. However, increasing the number of cohesive layers will increase the computational cost and the solution convergence may become rather complicated [13]. Since CFRP composites are essentially strain rate-independent in fibre-dominated modes such as on-axis $[0°,90°]_{2s}$ laminates subjected to in-plane tension and compression in the low-velocity (low strain-rate) regimes, the material constants obtained from the quasi-static tests (Table 2) were used in the FE models. Similarly, the cohesive law was assumed to be strain-rate insensitive, and thus static fracture-toughness values were assumed for a dynamic crack growth; this was proven to be sufficient in previous dynamic-fracture studies [22].

Cohesive-zone elements (CZEs) were used to model both the inter-ply and intra-ply damage modes and their interaction in CFRP laminates. The nominal quadratic stress criterion was used for damage initiation, whereas the Benzeggagh and Kenane criterion [23] was used for damage propagation. Parameters of the cohesive-zone elements presented in Table 3 were taken from the authors' previous work [17]. Apart from inter-ply damage modelling, CZEs have also been used to model intra-ply damage mechanisms such as splitting and ply fracture in composite laminates [16]. Here, the initiation of intra-ply fabric damage was linked to average ultimate flexural strength of 720 MPa in both warp and weft directions from the quasi-static bending tests. Intra-ply fracture evolution was based on fabric fracture energy of 40 kJ/m$^2$ in both warp and weft directions as reported in [10] for a similar carbon fabric. The stiffness of finite-thickness cohesive elements was calibrated according to $K = E_{33}/t_i$, proposed by Daudeville *et al.* [24], where $E_{33}$ (8 GPa) is the material's through-thickness stiffness and $t_i$ - 16 µm (taken from [25]) is the thickness of resin-rich interface between plies; resulting in interface stiffness of 5 x 10$^{14}$ N/m$^3$ for inter-ply damage. However, stiffness of the interface elements defined for intra-ply fracture was based on the longitudinal elastic stiffness $E_{11}$ of the ply instead of $E_{33}$ in the above relation resulting in a higher value of 1x10$^{15}$ N/m$^3$. Further details of the FE modelling such as the modelled test set-up, geometry, mesh and element types, and boundary conditions can be seen elsewhere [25].

### 3.2. Discussion of simulations results

#### 3.2.1. Response of damaged specimen

Comparison of the experimental and predicted force-time responses and evolution of damage at the impact location of of CFRP laminate in FE Model I at impact energy of 0.5 J is shown in Fig. 7. Fluctuations in the experimental force-time history designated as $F_d$ - Exp representing the internal damage initiation (load drops in Fig. 7) are observed before the peak load is reached. Apparently, both the global response and the contact duration are reasonably well predicted for the damaged specimen. However, the numerical damage threshold $F_d$ - FE, at which a significant change in the laminate stiffness was detected, was under-predicted in the FE model. This discrepancy might be due to the meso-level formulation for the plies in the model. Apparently, in experiments, the fabric-reinforced laminates absorbed more energy due to the ductile resin-rich pockets and the interlacing of fibres in two orthogonal directions, and, thus, offered more resistance to damage initiation, which were not taken into account in the simulations. However, in Fig. 7, the impact force and duration in numerical simulations are higher

than those in experiments, asserting higher energy dissipation in the FE model. This extra energy could be caused by an exaggerated amount of viscous dissipation in the model after damage initiation.

Similarly, the evolution of damage area at the impact location calculated with Model I is also plotted in Fig. 7. Figure 8 shows the calculated delamination area at three interfaces – FCL, MCL and BCL – in simulation with Model I at two different time intervals: at 3 ms (after $F_d$ - FE; Fig. 7) and at 6 ms (near peak load; Fig. 7). Here, delamination initiated first at the point of striker impact and then at the bending location of the cantilevered CFRP specimen. The ends of the trace were damaged more due to sharp corners of the hammer striker. A large and quick increase in the delamination area was observed simultaneously in all the layers beyond the time corresponding to $F_d$ - FE. It can be seen from both Figs. 7 and 8 that the largest area of delamination occurred at the mid-plane interface layer MCL due to the high level of through-thickness shear stress. Thus, a Mode-II type delamination initiated in the specimen's mid-region, where shear stress reached the interface shear strength, and grew more in MCL than FCL and BCL at the impact location. Similarly, the maximum bending stresses at the upper (front) and lower (back) plies were foremost responsible for damage formation at FCL and BCL of the specimen, especially at the bending location (Fig. 8). After the load peak was reached at 6 ms, the damage growth stopped in the unloading region of the load-time response (Fig. 7). The size and shape of the individual delaminations could not be compared to their experimental counterparts as such experimental results were not possible with the micro-CT for the full-scale specimen due to the requirement of field of view of the system. Also, due to the weaving architecture of the laminate, the spread of the damage is not in a 2D plane. Here, the in-situ quantification of various damage modes is either very cumbersome or non-feasible.

The main focus of the FE study is to compare and analyse the salient features of the dynamics and damage evolution in flexural (cantilevered) and quasi drop weight tests (two ends fixed) specimens. The load history and evolution of damage with time for Model II, where the specimen was constrained as a fixed-fixed beam, is presented in Fig. 9. The fixed-fixed boundary conditions increased the flexural rigidity of thin laminates resulting in a high peak of the impact force - 600 N, which is approximately 7.5 times more than that predicted with only one end fixed (cantilevered) specimen (see Fig. 7). The impact duration also reduced from 12 ms to 2.5 ms due to increased stiffness of the fixed-fixed specimen. Figure 10 shows the extent of delamination area at three interfaces – FCL, MCL and BCL – in simulations with Model II for fixed-fixed specimen at two different time intervals: at 0.2 ms (just at $F_d$ - FE; Fig. 9) and at

1.2 ms (near peak load; Fig. 9). Here, the damage pattern is also different due to the constraints. Due to the higher impact force, the extent and magnitude of damage at the impact location are higher especially near the constrained top edge than that shown in Fig. 8. Here, too, the MCL is more damaged at the impact location.

To investigate the effect of constraints on inter-ply damage evolution, comparison of damage progression in both Models I and II with cantilevered and both ends fixed (quasi drop weight, qDW) conditions, respectively, is presented in Fig. 11. The rate of damage growth in quasi drop weight specimen is faster than that of cantilevered one. This demonstrates that due to both ends fixed, the specimen of the same size under similar impact energy of 0.5 J dissipates a lot of energy very quickly than the cantilevered specimen in Model I. Further, the extent of damage is also higher in quasi drop weight model in all interface layers than that of cantilevered specimen. Here, it can be inferred from these results that the boundary conditions of the specimens has not only a significant effect on the impact force and duration but also on the damage evolution within the specimen.

**3.3.2. Response of fractured specimen**

Fabric fracture occurred as the impact energy was increased to 0.6 J in experimental tests. The predicted evolution of impact force in Model III is compared with experimental results at this level of energy in Fig. 12. Here, too, the load drops designated as $F_d$ - Exp and $F_d$ - FE represents delamination initiation for the experiments and numerical results, respectively. The experimental curve shows more fluctuations due to significant damage after the damage threshold $F_d$ - Exp at higher impact energy, followed by the ultimate ply fracture at 4.8 ms. The final ply fracture is presented by a sudden drop in the impact force; however, the load didn't drop to zero, because in dynamic bending the distal plies in compression were not fractured causing a residual load of about 22 N. The simulation showed the ply fracture somewhat earlier - at 4.38 ms, which might be due to the low ply fracture initiation strength defined in Model III. Still, the FE analysis gave a good prediction of the important characteristics of the failure process.

The sequence of inter-ply delamination and intra-ply fabric breakage as well as their interaction in Model III is illustrated in the deformed contour plots for flexural stress $\sigma_{11}$ shown in Fig. 13. Although the laminate was fully delaminated in Fig. 13a, the flexural stress contours were almost uniform. The stress reduced as the first ply's fracture occurred at 4.38 ms as shown in Fig. 13b followed by fracture of the second ply in Figs. 13c at 4.62 ms. The third and fourth plies remained intact because of compressive

stresses on back side of the specimen in the bending. These plies carried the residual load and were in tension and compression states, respectively, as can be seen in Figs. 13c and d. Stress concentration at the locations of inter-ply and intra-ply crack tips is apparent in Figs. 13b-d. As the load increased, the ply elements moved relative to each other as in Mode-II type fracture along the delaminated interface layers as shown in Fig. 13d. There may be the possibility of fibre kinking due to buckling instability in the back plies under compression; however, this behaviour is not studied in the meso-scale models.

## 4. Conclusions

The behaviour of fabric-reinforced composites under dynamic bending was studied using experimental tests, micro-CT scanning and numerical simulations. The dynamic tests revealed that the CFRP laminates were fractured at lower energy levels than GFRP due to their lower energy absorbing capability. However, the impact strength of the CFRP laminates was higher than that of GFRP. Further, on-axis GFRP laminates exhibited a strain-rate sensitive behaviour as compared to CFRP specimens. In the impact bending tests, the specimens failed at lower impact energy as compared to their failure in drop weight impact tests. It was also found that damage in the specimens at the impact location was from its front to the back in the large-deflection impact tests, unlike the bottom-to-top character in drop weight tests. Considerable matrix cracking leading to tow debonding and delamination was observed along with tow fibre fracture in the micro-CT scanning of the impacted CFRP laminates. This microstructural characterisation formed a basis for damage incorporation in the developed 3D FE models.

The results of meso-scale 3D FE models of CFRP laminates were close to the experimental ones, and, the simulations were capable to reproduce the damage sequence and patterns observed experimentally. The numerical models helped to offer significant information about the complex damage phenomena that occurred at various stages of impact bending. For instance, interaction of delamination and ply fracture, which cannot be assessed directly in real tests and by non-destructive investigation, was captured with the CZM-based modelling approach. Similarly, the effect of boundary conditions on the dynamic response was also predicted for the first time, which is hard to obtain experimentally for the fixed-fixed conditions. Such conditions resulted in an increased flexural rigidity of the impacted specimen and the higher peak load and reduced impact duration. These quasi drop weight test conditions also resulted in a larger extent of damage with a faster growth rate. This also corroborated our observations that cantilever specimens failed at lower impact energies than fully clamped specimens in drop weight impact tests.

**References**

[1] Sutcliffe MPF, Monroy Aceves C, Stronge WJ, Choudhry RS, Scott AE. Moderate speed impact damage to 2D-braided glass–carbon composites. Composite Structures. 2012;94(5):1781-1792.

[2] Naik N, Chandra Sekher Y, Meduri S. Damage in woven-fabric composites subjected to low-velocity impact. Composites Science and Technology. 2000;60(5):731-744.

[3] Crabtree P, Dhokia V, Newman S, Ansell M. Manufacturing methodology for personalised symptom-specific sports insoles. Robotics and Computer-Integrated Manufacturing. 2009;25(6):972-979.

[4] http://www.ossur.com. 2013.

[5] Menna C, Asprone D, Caprino G, Lopresto V, Prota A. Numerical simulation of impact tests on GFRP composite laminates. International Journal of Impact Engineering. 2011;38(8–9):677-685.

[6] Scott A, Mavrogordato M, Wright P, Sinclair I, Spearing S. In situ fibre fracture measurement in carbon–epoxy laminates using high resolution computed tomography. Composites Science and Technology. 2011;71(12):1471-1477.

[7] Sket F, Seltzer R, Molina-Aldareguía J, Gonzalez C, LLorca J. Determination of damage micromechanisms and fracture resistance of glass fiber/epoxy cross-ply laminate by means of X-ray computed microtomography. Composites Science and Technology. 2012;72:350-359.

[8] Ullah H, Harland A, Silberschmidt V. Experimental and Numerical Analysis of Damage in Woven GFRP Composites Under Large-deflection Bending. Applied Composite Materials. 2012;19(5):769-783.

[9] Aktaş M, Ersen Balcıoğlu H, Aktaş A, Türker E, Emin Deniz M. Impact and post impact behavior of layer fabric composites. Composite Structures. 2012;94:2809-2818.

[10] Iannucci L, Willows M. An energy based damage mechanics approach to modelling impact onto woven composite materials--Part I: Numerical models. Composites Part A: Applied Science and Manufacturing. 2006;37(11):2041-2056.

[11] Kim JK, Sham ML. Impact and delamination failure of woven-fabric composites. Composites Science and Technology. 2000;60(5):745-761.

[12] Wisnom MR, Hallett SR. The role of delamination in strength, failure mechanism and hole size effect in open hole tensile tests on quasi-isotropic laminates. Composites Part A. 2009;40(4):335-342.

[13] Ullah H, Harland AR, Lucas T, Price D, Silberschmidt VV. Finite-element modelling of bending of CFRP laminates: Multiple delaminations. Computational Materials Science. 2012;52(1):147-156.

[14] Wisnom MR. Modelling discrete failures in composites with interface elements. Composites Part A. 2010;41(7):795-805.

[15] Fang XJ, Zhou ZQ, Cox BN, Yang QD. High-fidelity simulations of multiple fracture processes in a laminated composite in tension. Journal of the Mechanics and Physics of Solids. 2011;59(7):1355-1373.

[16] Hallett SR, Jiang WG, Khan B, Wisnom MR. Modelling the interaction between matrix cracks and delamination damage in scaled quasi-isotropic specimens. Composites Science and Technology. 2008;68(1):80-89.

[17] Ullah H, Harland AR, Silberschmidt VV. Damage modelling in woven-fabric CFRP laminates under large-deflection bending. Computational Materials Science. 2012;64:130-135.

[18] Hosur M, Adbullah M, Jeelani S. Studies on the low-velocity impact response of woven hybrid composites. Composite Structures. 2005;67(3):253-262.

[19] López-Puente J, Li S. Analysis of strain rate sensitivity of carbon/epoxy woven composites. International Journal of Impact Engineering. 2012;48(0):54-64.

[20] Sokolinsky VS, Indermuehle KC, Hurtado JA. Numerical simulation of the crushing process of a corrugated composite plate. Composites Part A: Applied Science and Manufacturing. 2011;42:1119-1126.

[21] Lopes C, Camanho P, Gürdal Z, Maimí P, González E. Low-velocity impact damage on dispersed stacking sequence laminates. Part II: Numerical simulations. Composites Science and Technology. 2009;69(7-8):937-947.

[22] Gözlüklü B, Coker D. Modeling of the dynamic delamination of L-shaped unidirectional laminated composites. Composite Structures. 2012;94(4):1430-1442.

[23] Benzeggagh ML, Kenane M. Measurement of mixed-mode delamination fracture toughness of unidirectional glass/epoxy composites with mixed-mode bending apparatus. Composites Science and Technology. 1996;56(4):439-449.

[24] Daudeville L, Allix O, Ladeveze P. Delamination analysis by damage mechanics: some applications. Composites Engineering. 1995;5(1):17-24.

[25] Ullah H, Harland AR, Silberschmidt VV. Damage and fracture in carbon fabric reinforced composites under impact bending. Composite Structures. 2013;101(0):144-156.

**Figure Captions**

Fig. 1. Resil impact test set-up

Fig. 2. Experimental response of twill 2/2 CFRP laminates at various impact energies: (a) force-time curves; (b) force-deflection curves

Fig. 3. Experimental response of twill 2/2 GFRP laminates at various impact energies: (a) force-time curves; (b) force-deflection curves

Fig. 4. Reconstructed 3D tomographs of twill 2/2 CFRP specimen at impact location across height of sample (resolution 6.7 μm): (a) edge; (b) 25% (1 mm above impact centre line) (c) 50% (at impact centre); (d) 75% (below impact centre line) of height

Fig. 5. Reconstructed 3D tomographs of twill 2/2 CFRP specimen at bending (fracture) location across width of sample (resolution 6.1 μm): (a) edge; (b) 25%; (c) 50%; (d) 75% of width

Fig. 6. Schematics of FE models for cantilever bending (Model I) (a), fixed-fixed bending ( quasi drop weight test simulation) (Model II) (b) and fractured (Model III) (c) behaviours of CFRP specimens tested at 0.5 J and 0.6 J impact energy, respectively

Fig. 7. Comparison of experimental and numerical force-time response and evolution of inter-ply delamination area at the impact location of CFRP laminate in FE Model I at impact energy of 0.5 J

Fig. 8. Delamination evolution in FE Model I at impact energy of 0.5 J at 3 ms (a) and 6 ms (b) [25]

Fig. 9. Numerical force-time response and damage evolution in FE Model II with fixed-fixed boundary (quasi drop weight (qDW) test) conditions at impact energy of 0.5 J

Fig. 10. Delamination evolution in FE Model II with fixed-fixed boundary conditions of the specimen at impact energy of 0.5 J at 0.2 ms (a) and 1.2 ms (b)

Fig. 11. Comparison of damage evolution under cantilever (flexural) and fixed-fixed (qDW) conditions of CFRP laminates from FE Models I and II at 0.5 J impact energy, respectively

Fig. 12. Comparison of experimental and numerical (Model III) force-time response for CFRP laminates at impact energy of 0.6 J

Fig. 13. Contours of bending stress $\sigma_{11}$ in Model III showing interaction of inter-ply and intra-ply damage at impact energy of 0.6 J at 4.2 ms (a), 4.38 ms (b), 4.62 ms (c) and 6.0 ms (d) (side view; scaling factor 0.5; fractured interfaces are represented by white colour)

**Table captions**

Table 1. Parameters of twill 2/2 woven composites

Table 2. Material properties of twill 2/2 woven composites

Table 3. Material parameters of inter-ply cohesive elements

**Table 1**

Table 1. Parameters of twill 2/2 woven composites

| | | |
|---|---|---|
| Fibre Type | Carbon T200 | Glass |
| Filament diameter (μm) | 7.0 | 9.0 |
| Yarns | 3000 | 3x68 |
| End/pick count, yarns/cm | 5.2/5.14 | 7.0/9.52 |
| Fabric areal density ($g/m^2$) | 200 | 290 |
| Polymer | Thermoplastic polyurethane (TPU) | Thermoplastic polyurethane (TPU) |
| Laminate density ($g/cm^3$) | 1.47 | 1.82 |
| Fibre volume fraction (%) | 45 | 45 |
| Number of layers | 4 | 4 |
| Ply thickness (mm) | 0.25 | 0.25 |

**Table 2**

Table 2. Material properties of twill 2/2 woven composites

| | $E_{11}$ (GPa) | $E_{22}$ (GPa) | $E_{33}$ (GPa) | $G_{12}$ (GPa) | $G_{13}$=$G_{23}$ (GPa) | $v_{12}$ |
|---|---|---|---|---|---|---|
| CFRP | 55.0 | 52.0 | 8.0 | 3.8 | 3.7 | 0.05 |
| GFRP | 21.5 | 21.0 | 8.5 | 3.1 | 4.1 | 0.11 |

**Table 3**

Table 3. Material parameters of inter-ply cohesive elements

| | Mode I | Mode II |
|---|---|---|
| Normalised elastic modulus ($N/m^3$) | $5 \times 10^{14}$ | $5 \times 10^{14}$ |
| Inter-ply strength (MPa) | 12 | 26 |
| Inter-ply fracture toughness ($kJ/m^2$) | 0.8 | 1.75 |

**Figure 1 - new**

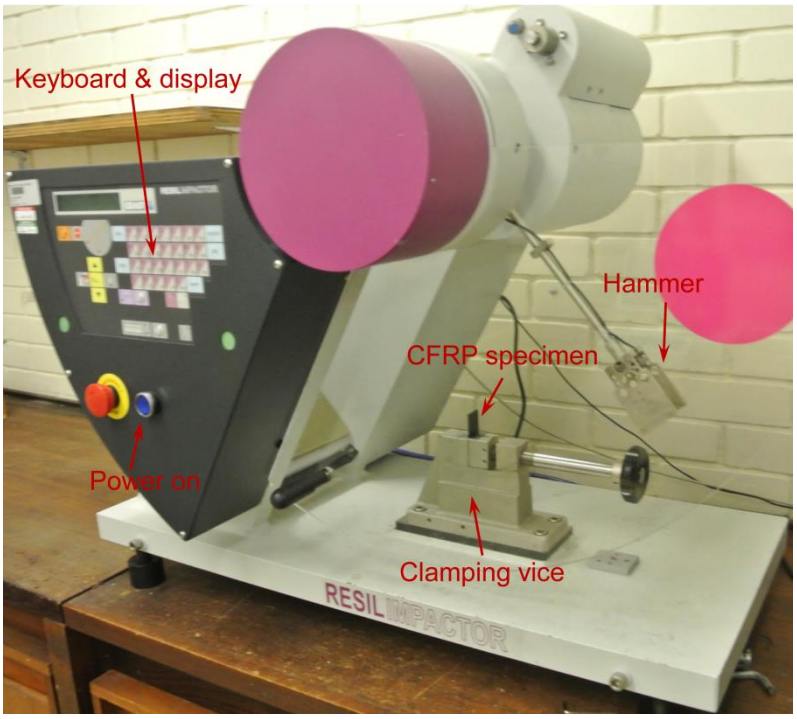


Fig. 1. Resil impact test set-up

**Figure 2**

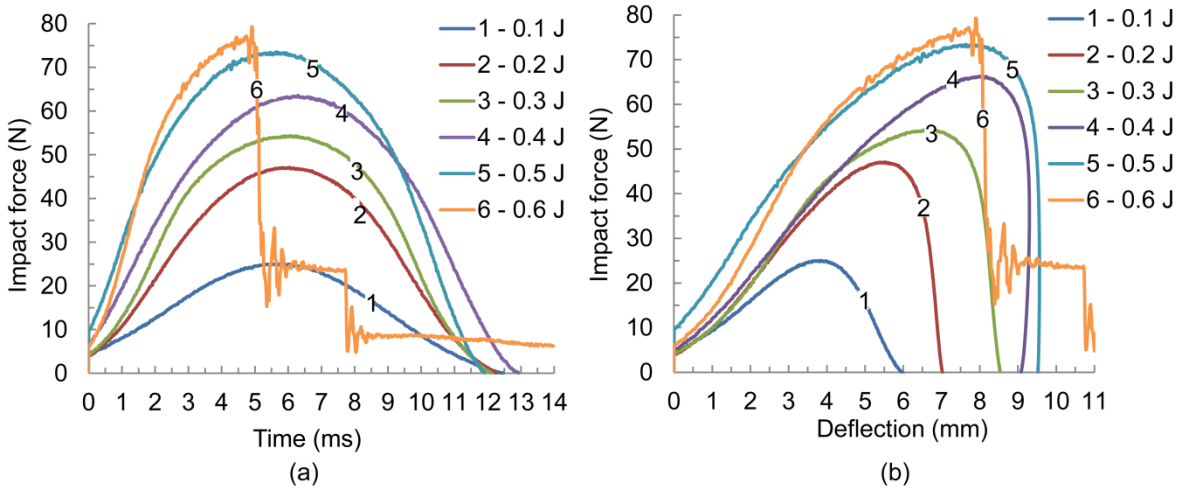
Impact force (N)
Time (ms)
(a)
Deflection (mm)
(b)
1 - 0.1 J
2 - 0.2 J
3 - 0.3 J
4 - 0.4 J
5 - 0.5 J
6 - 0.6 J

**Figure 3**

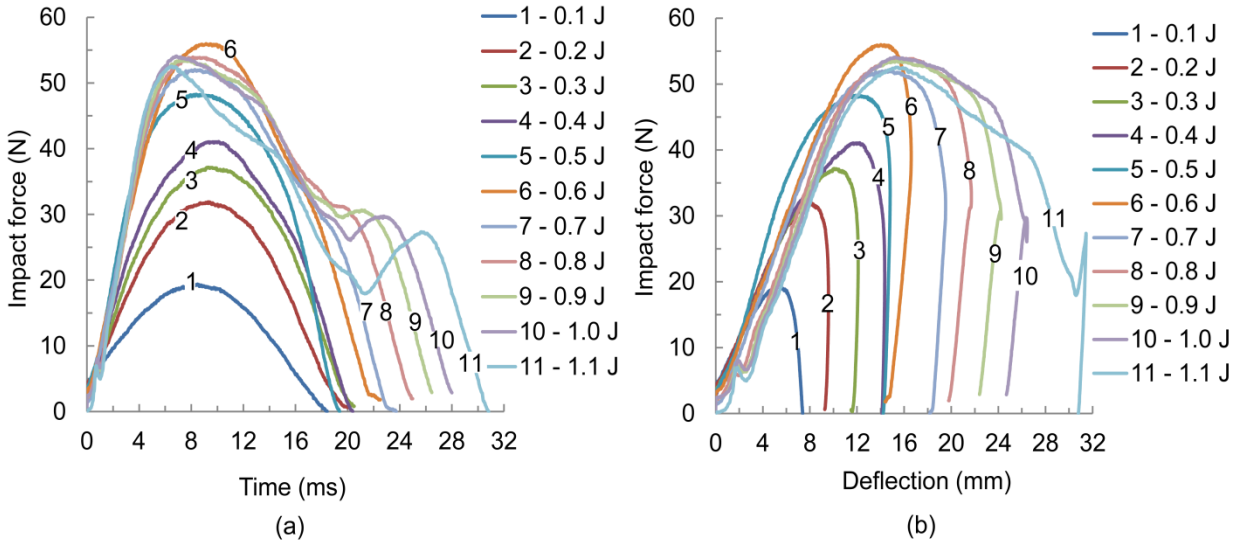
Impact force (N)
Time (ms)
(a)
Deflection (mm)
(b)
1 - 0.1 J
2 - 0.2 J
3 - 0.3 J
4 - 0.4 J
5 - 0.5 J
6 - 0.6 J
7 - 0.7 J
8 - 0.8 J
9 - 0.9 J
10 - 1.0 J
11 - 1.1 J

**Figure 4**

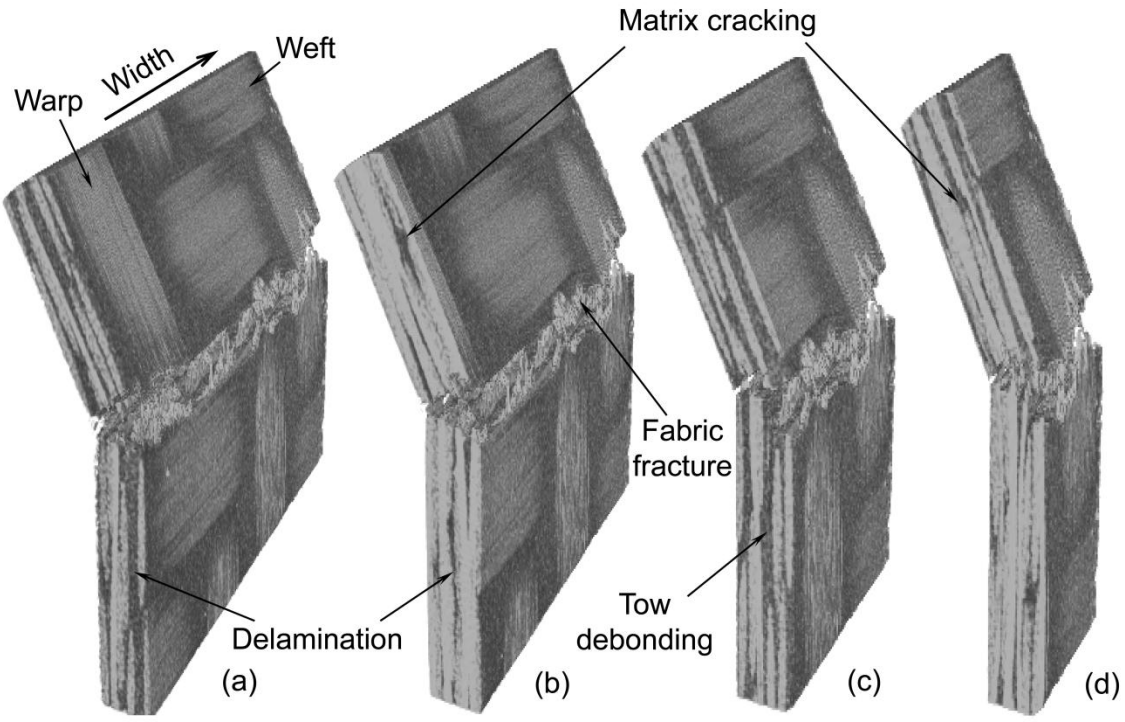
Warp
Width
Weft
Matrix cracking
Fabric
fracture
Tow
debonding
Delamination
(a)
(b)
(c)
(d)

**Figure 5**

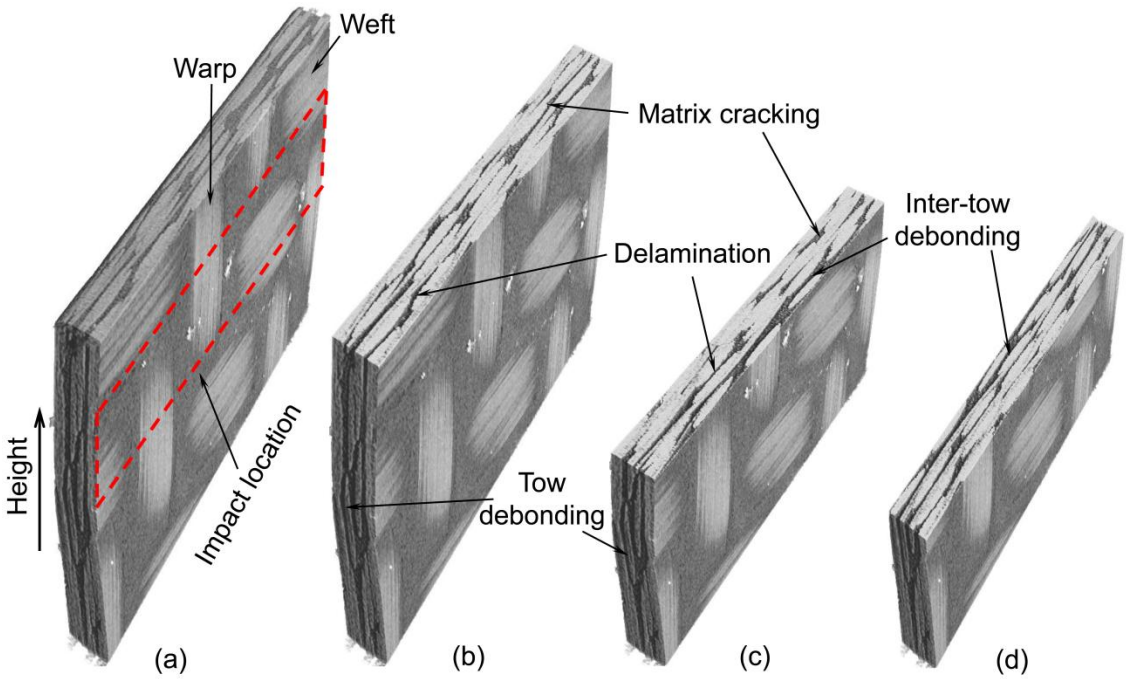
Weft
Warp
Height
Impact location
(a)
Matrix cracking
Delamination
Tow debonding
(b)
Inter-tow debonding
(c)
(d)

**Figure 6**

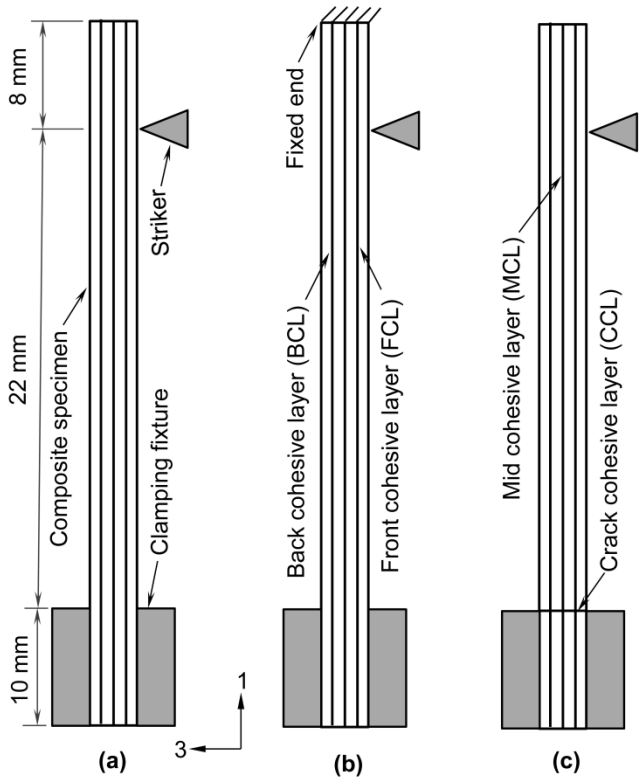
8 mm
22 mm
10 mm
Striker
Composite specimen
Clamping fixture
1
3
(a)
Fixed end
Back cohesive layer (BCL)
Front cohesive layer (FCL)
(b)
Mid cohesive layer (MCL)
Crack cohesive layer (CCL)
(c)

**Figure 7**

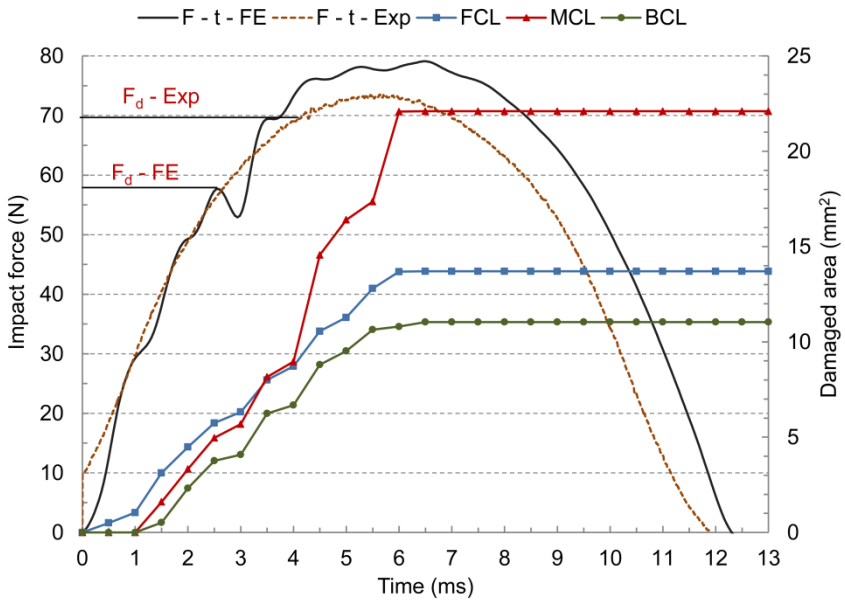
F - t - FE
F - t - Exp
FCL
MCL
BCL
$F_d$ - Exp
$F_d$ - FE
Impact force (N)
Damaged area (mm²)
Time (ms)
0
10
20
30
40
50
60
70
80
0
5
10
15
20
25
0
1
2
3
4
5
6
7
8
9
10
11
12
13

**Figure 8**

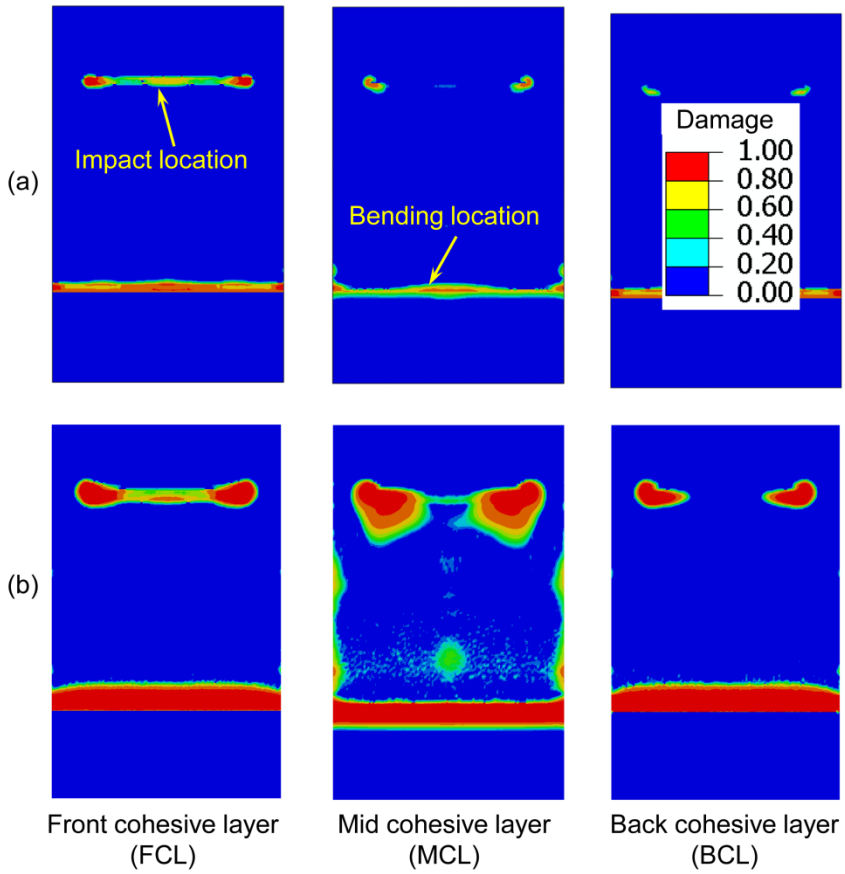
(a)
Impact location
Bending location
Damage
1.00
0.80
0.60
0.40
0.20
0.00
(b)
Front cohesive layer (FCL)
Mid cohesive layer (MCL)
Back cohesive layer (BCL)

**Figure 9**

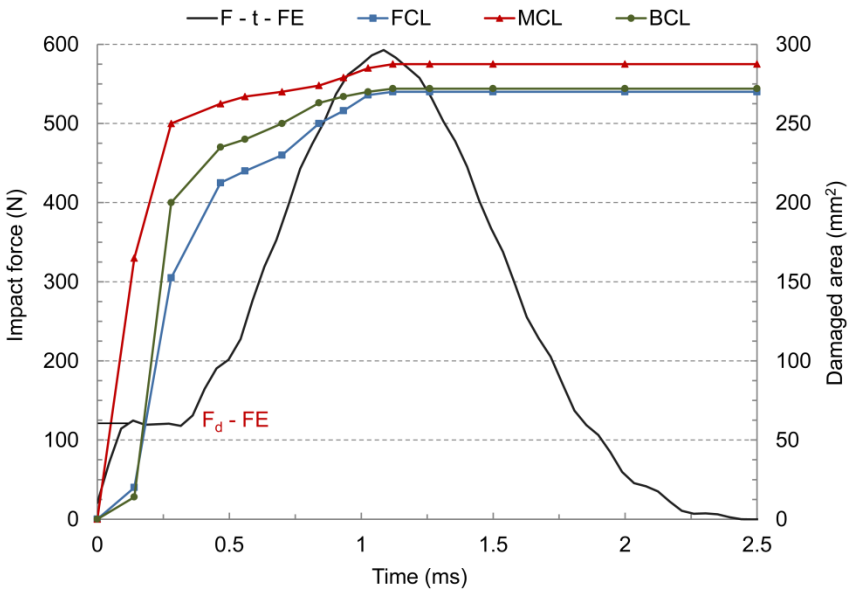
F - t - FE
FCL
MCL
BCL
600
500
400
300
200
100
0
300
250
200
150
100
50
0
0
0.5
1
1.5
2
2.5
Impact force (N)
Damaged area (mm²)
Time (ms)
F_d - FE

**Figure 10**

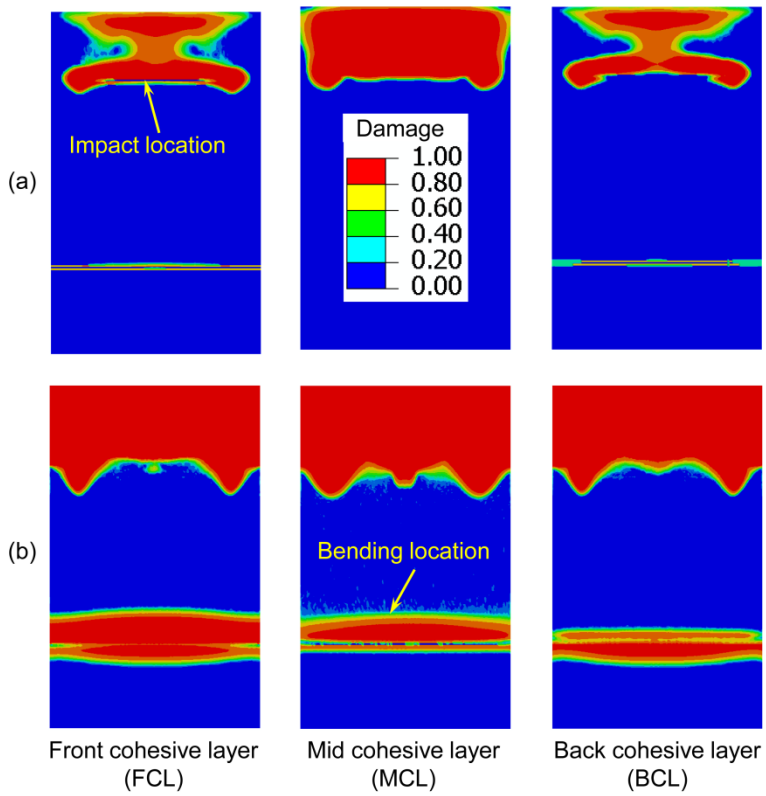
(a)
Impact location
Damage
1.00
0.80
0.60
0.40
0.20
0.00
(b)
Bending location
Front cohesive layer (FCL)
Mid cohesive layer (MCL)
Back cohesive layer (BCL)

**Figure 11**

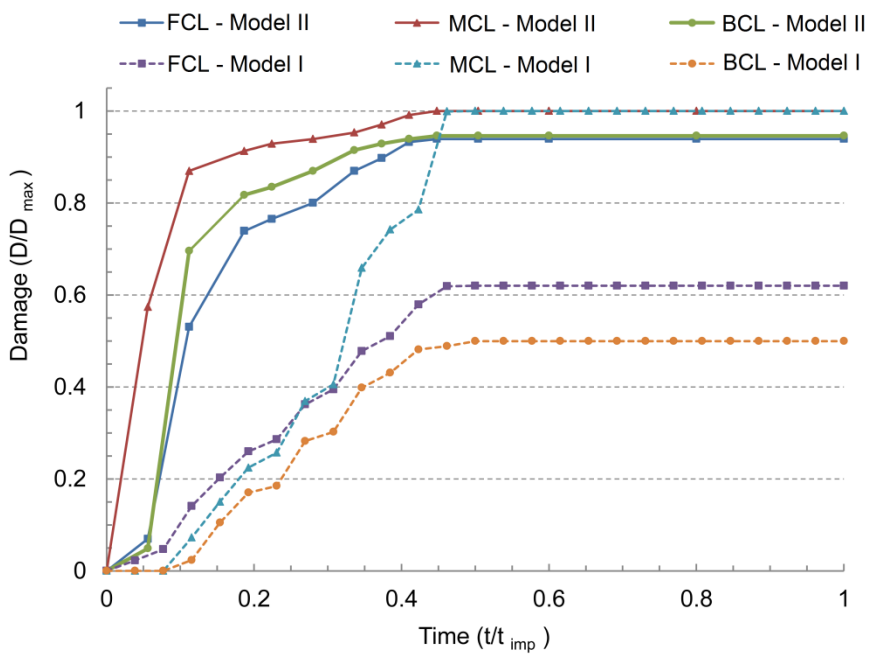
FCL - Model II
MCL - Model II
BCL - Model II
FCL - Model I
MCL - Model I
BCL - Model I
Damage (D/D max )
Time (t/t imp )
0
0.2
0.4
0.6
0.8
1

**Figure 12**

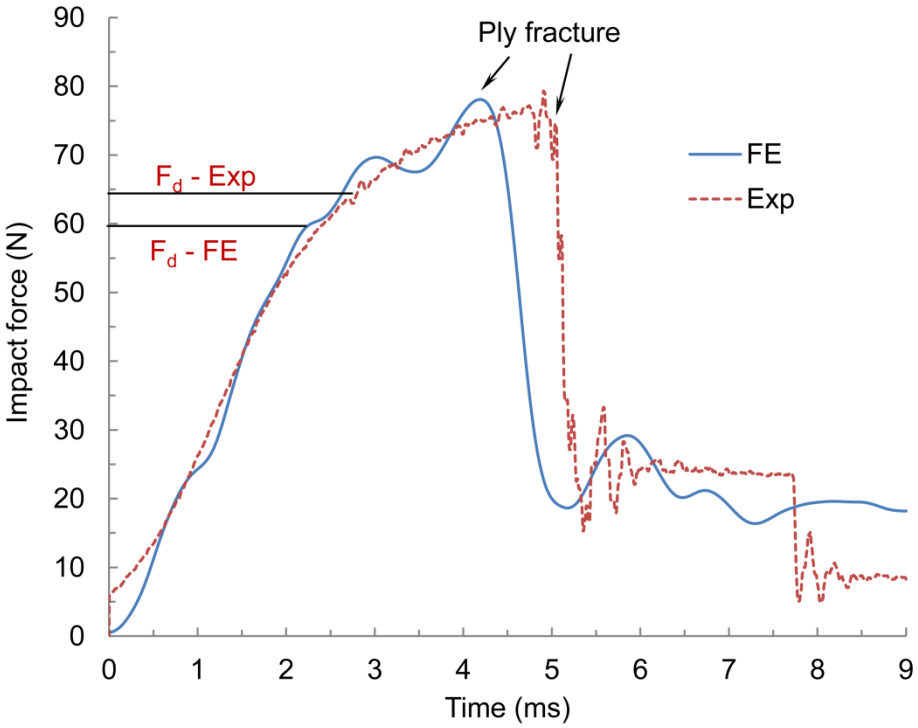
Ply fracture
FE
Exp
$F_d$ - Exp
$F_d$ - FE
Impact force (N)
Time (ms)
0
10
20
30
40
50
60
70
80
90
0
1
2
3
4
5
6
7
8
9

**Figure 13**

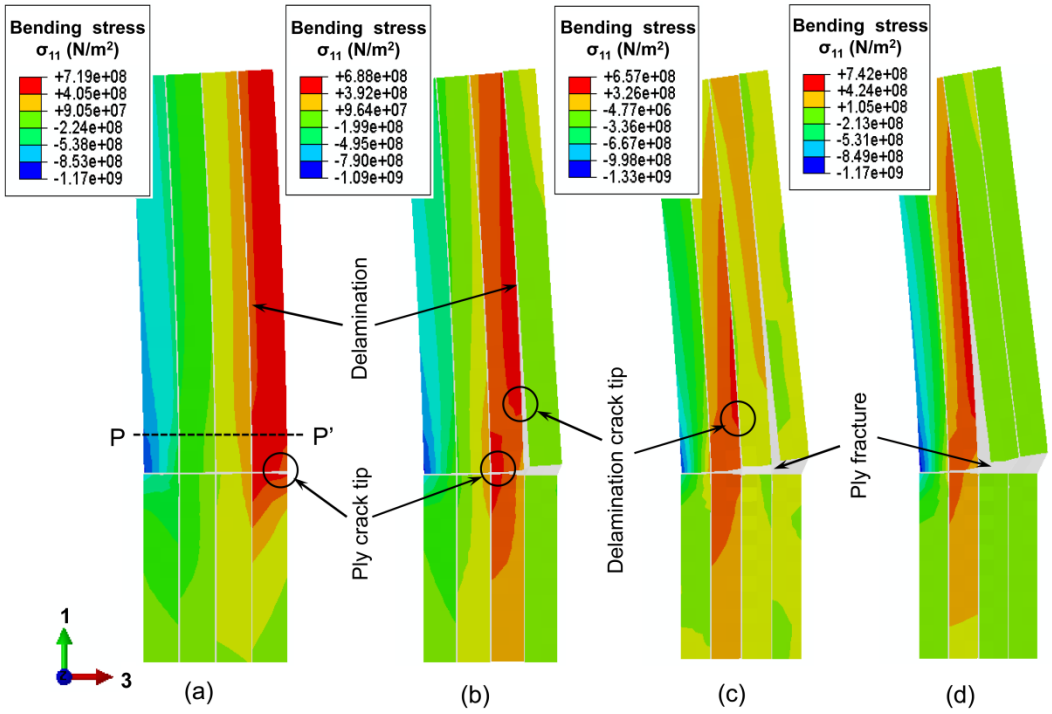
Bending stress
σ11 (N/m²)
+7.19e+08
+4.05e+08
+9.05e+07
-2.24e+08
-5.38e+08
-8.53e+08
-1.17e+09
Bending stress
σ11 (N/m²)
+6.88e+08
+3.92e+08
+9.64e+07
-1.99e+08
-4.95e+08
-7.90e+08
-1.09e+09
Bending stress
σ11 (N/m²)
+6.57e+08
+3.26e+08
-4.77e+06
-3.36e+08
-6.67e+08
-9.98e+08
-1.33e+09
Bending stress
σ11 (N/m²)
+7.42e+08
+4.24e+08
+1.05e+08
-2.13e+08
-5.31e+08
-8.49e+08
-1.17e+09
Delamination
P
P'
Ply crack tip
Delamination crack tip
Ply fracture
1
3
(a)
(b)
(c)
(d)